A New Strategy for Organic Optoelectronic Devices

Mihee Heo

Energy Conversion and Storage Major
Interdisciplinary School of Green Energy
Graduate School of UNIST

2011

A New Strategy for Organic Optoelectronic Devices

Mihee Heo

Energy Conversion and Storage Major
Interdisciplinary School of Green Energy
Graduate School of UNIST

A New Strategy for Organic Optoelectronic Devices

A thesis
submitted to the Interdisciplinary School of Green Energy
and the Graduate School of UNIST
in partial fulfillment of the
requirements for the degree of
Master of Science

Mihee Heo

06. 08. 2011
Approved by

Major Advisor
Jin Young Kim

A New Strategy for Organic Optoelectronic Devices

Mihee Heo

This certifies that the thesis of Mihee Heo is approved.

06. 08. 2011

signature

Thesis supervisor: Jin Young Kim

signature

Changduk Yang

signature

Soojin Park

Abstract

My MS research has focused on alternative organic optoelectronic devices as promising technology that may be environmentally friendly renewable energy resources and the next generation flat-panel display platform. During my research, first, high-performance organic optoelectronic devices enhanced by surface plasmon resonance have been demonstrated containing interfacial metal nanoparticles such as copper, gold, and copper-gold alloy between indium tin oxide (ITO) and poly(3,4-ethylenedioxylenethiophene):polystyrene sulfonic acid (PEDOT:PSS) via a polystyrene-*block*-poly(2-vinylpyridine) (PS-*b*-P2VP) copolymer template. In the organic solar cells (OPVs), the improved optical absorption is attributed to the increased electric field in the photoactive layer caused by excited localized surface plasmon from the nanoparticles. Moreover, enhanced luminance intensity and improved luminous efficiency in organic light emitting diodes (OLEDs) are achieved due to the acceleration of the radiative processes at the surface plasmon frequency. A significant effect of the SPR is attained in organic optoelectronic devices, which show up to 20% enhanced performance as compared with reference devices. Second, a rod-coil block copolymer consisting of poly(3-hexylthiophene) (P3HT) and poly(*N*-vinylcarbazole) (PVK) (P3HT-b-PVK) in a single molecular architecture is prepared as the first example for white light emitting diodes(WOLEDs). By obtaining the phase separated domains in thin film of the resulting block copolymer, it is possible to suppress energy transfer from PVK as wide bandgap units to P3HT as low bandgap blocks, yielding dual emissions for white electroluminescence with CIE coordination of (0.34, 0.33).

Contents

List of Figures

List of Tables

CHAPTER 1
INTRODUCTION

1.1 The Optoelectronic Devices

The increasing demand for energy and involving environmental problem over the past several decades has resulted in a drive for research into possible renewable energy sources that are both commercially viable and do not create waste products that are detrimental to the environment. The solar energy that reaches the earth's surface is the largest carbon-free clean energy source, which could be harvested with photovoltaic cells that generate useful electric energy from sun light through multiple steps of energy conversion processes.

Current solar cell markets based on inorganic silicon are environmentally clean, but expensive, even though they have relatively high power conversion efficiencies.[1] Due to this problem, organic solar cells are in the spotlight as a next generation renewable energy sources.

Organic based solar cells (OSCs) have great advantages of easy fabrication, low cost, and mechanically flexible photovoltaic devices over a large area.[2,3] Significant efforts have been done in recent years to improve the efficiency of PSCs using a variety of different processing strategies such as a well-understanding of device physics,[4-6] new materials for high-performance,[7-9] optimization of morphologies by an advanced processing methods,[10-12] and device architectures.[13,14] However, the power conversion efficiency is not enough yet up to the level for commercialization and further enhancement is still required for practical applications.

All types of lighting account for about 22 percent of the nation's electricity consumption with 40 percent of that amount consumed by inefficient incandescent lamps which have only energy conversion efficiency of 10 percent. About 90 percent of the energy goes to the production of heat. Fluorescent lamps have 70 percent conversion efficiency but still a significant amount of the used energy is wasted.[15] Not much progress has been done in the energy efficiency of all the conventional light sources within the past fifty decades.

In recent years, one of the new emerging light technologies which have the potential of becoming more energy-efficient than the existing light sources is the organic light emitting diodes (OLEDs) combined with low cost, lightweight, easily processable and high throughput manufacturability. In the area of OLEDs, in particular, white organic light emitting diodes (WOLEDs) have been attracting more and more attention due to their potential applications in backlights for flat-panel displays and solid-state lighting sources.[16,17]

A lot of researches have been devoted to developing WOLEDs, for example, stacking the multi

emissive layers in a single device structure,[18,19] using doped or blended polymeric system with different fluorescent or phosphorescent materials.[20-22]

1.1.1 The Photovoltaic Effect

The photovoltaic effect is the creation of a voltage or a corresponding electric current in a material upon exposure to radiation in light which is made up of packets of energy, called photons. The photovoltaic effect is different in that the generated electrons are transferred from the valence to conduction bands within the material, resulting in the buildup of a voltage between two electrodes. In the solar spectrum, only 45 percent of incident light energy is in the visible light range, while around 50 percent is in the infrared range (IR). The photons in ultraviolet (UV) and visible range have enough energy to pump electrons between different bands in semiconducting material, and this can be effectively used for charge generation. On the other hand, not enough energy is provided in IR waves to excite electrons. (**Figure 1.1**)

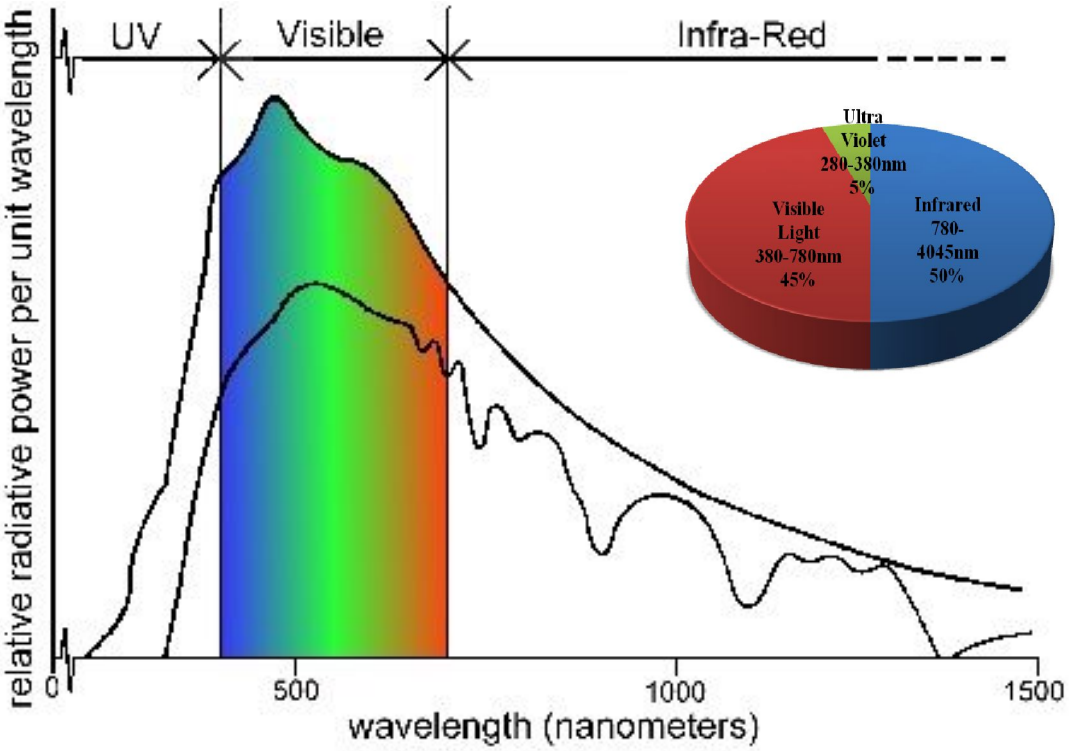

Figure 1.1. Solar spectrum and its distribution.

The discovery of the photovoltaic effect is commonly ascribed to Becquerel, a French physicist who discovered that certain materials produced small amounts of photocurrent when platinum electrodes covered with silver bromide or silver chloride was illuminated in aqueous solution.[23] Albert Einstein explained the photoelectric effect in 1905, where blue or ultraviolet light provides enough energy for electrons to escape completely from the metal surface, which established the foundation for a theoretical understanding of the photovoltaic effect.

In most cases, when light is absorbed by matter, photons are given up to excited electrons to higher energy states within the material, but the excited electrons promptly relax to the ground state, while there is some built-in difference which pulls the excited electrons away before they can relax back in the photovoltaic devices. (**Figure 1.2**)

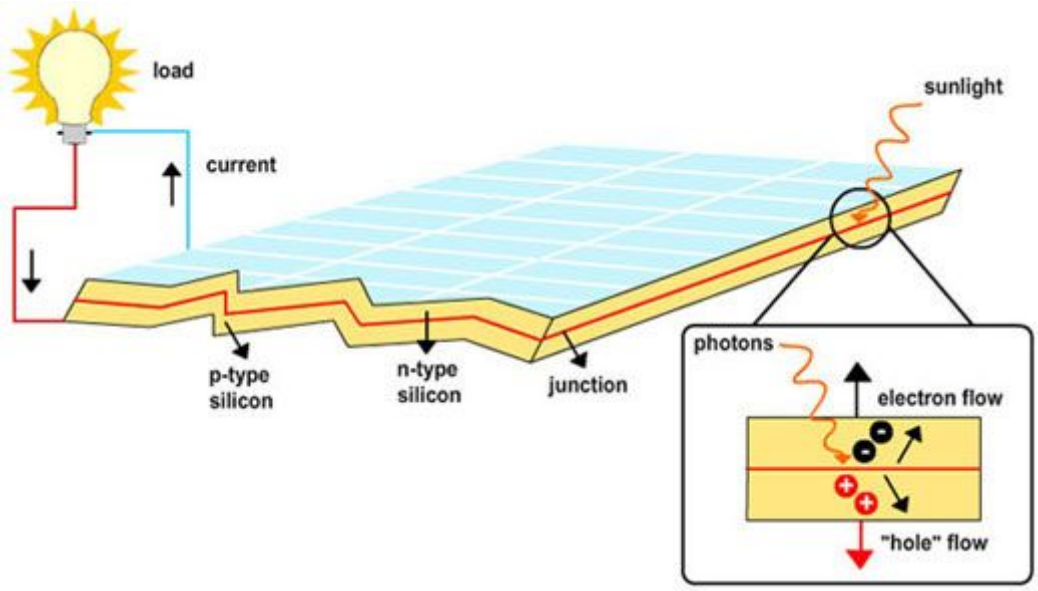

Figure 1.2. Photovoltaic effect.

The photovoltaic process is composed of following four steps: light absorption, charge generation, charge transport, and charge collection. Light absorption occurs when the material has a semiconducting property that responds to incident light. After that the incident photon hits electrons at the ground state, semiconductor materials create free carriers and they slightly relax and form an exciton which consists of a bounded electron and hole pair. The dissociation of this electron-hole pair produces free charge carriers which are transported through their respective phases to the electrodes in order to be extracted.

1.1.2 Electroluminescence

Electroluminescence (EL) is a phenomenon in which a material emits light involving non-thermal generation when electricity is passed through it as shown in **Figure 1.3**. This process is the result of radiative recombination of electrons and holes in a semiconductor material. Before recombination, electrons and holes may be separated either by doping the material to form a p-n junction or through excitation by impact of high-energy electrons accelerated by a strong electric field. When injected electrons and holes are recombined by the application of an external electric field in a material, these pairs relax to the ground state and release their energy with radiation of light, called photons. Electroluminescence is one of the greatest discoveries of the twentieth century, which is first founded for inorganic materials in 1936 by Destiriau.[24] By using this process, the devices are fabricated using thin films of either organic or of inorganic materials which contain a host material or bulk semiconductor and a dopant of the visible color emitted.

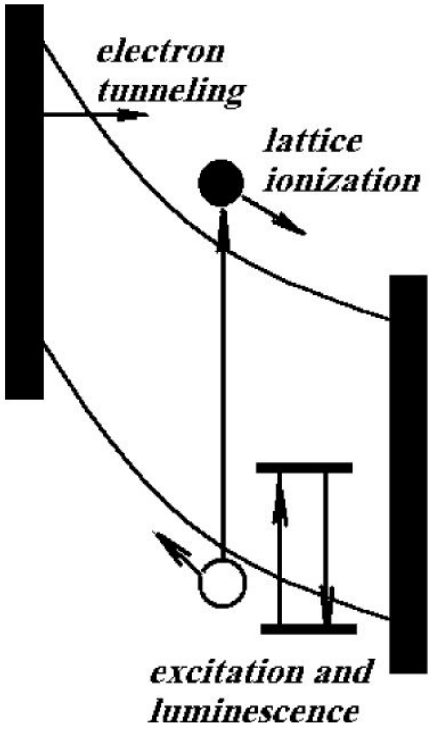

Figure 1.3. Principles of operation of a thin film electroluminescent device.

1.2 The History of Optoelectronic Devices

1.2.1 The Photovoltaic Cells

The first report of photovoltaic effect is ascribed to Becquerel in 1839 when he discovered that a photocurrent on a silver coated platinum electrode immersed in electrolyte. In 1876, Adams and his coworker made the first reports on solid state photovoltaic devices which were produced in a sample of selenium when contacted by two heated platinum contacts.[25] They founded that a current was produced spontaneously by light without any external power supply. In 1894, Fritts developed the first large-area photovoltaic device by a layer of selenium between gold and another metal. Anthracene was the first organic compound in which photoconductivity was observed by Pochettino in 1906.[26] During the 1930s, the theory of metal- semiconductor barrier layers was developed by Walter Schottly, called Schottly barrier devices.

In the 1950s, the significant development of silicon electronics followed a way to manufacture *p-n* junction in silicon PV cells achieved significant improvement of efficiency with first practical application. In 1954, by Chapin, Fuller and Pearson at Bell Laboratories, the first silicon solar cell was reported with an efficiency of 6%.[27] Also in same year, a cadmium sulphide *p-n* junction was produced with an efficiency of 6%. Today Si-based solar cells are by far the most dominating type of PVs used and account for 99% of all PVs.

In the 1970s, the energy supply crisis led to a sudden growth of interest in alternative sources of energy. With this trend, PVs had attracted considerable interest. Research focused on developing device physics and process technology. Methods to reduce the production costs of thin film technologies using amorphous silicon or microcrystalline silicon were also actively investigated. Additionally, research into tandem cell structures and band gap tuning of semiconducting materials was conducted during this period to improve power conversion efficiency.

In 1990s, interest in PVs increasingly expanded due to the awareness of the need to new energy sources alternative to fossil fuels along with the environmental issues related to global warming. In the early 2000s, PV technology has begun to impact the world by encouraging the expansion of energy resources from oil to green energy.

In the field of organic solar cells, after discovery of organic dyes in 1960s, Tang realized bi-layer PV device consisting of CuPC and a perylene derivative with efficiency of 1 percent.[28] In the early 2000s, Alan J. Heeger and his coworkers won the Nobel Prize on establishment of organic semiconductor.[29] From their findings, organic materials have been a subject of intense interest for new future of PV technology. This discovery has prompted a lot of active researches. (**Figure 1.4**)

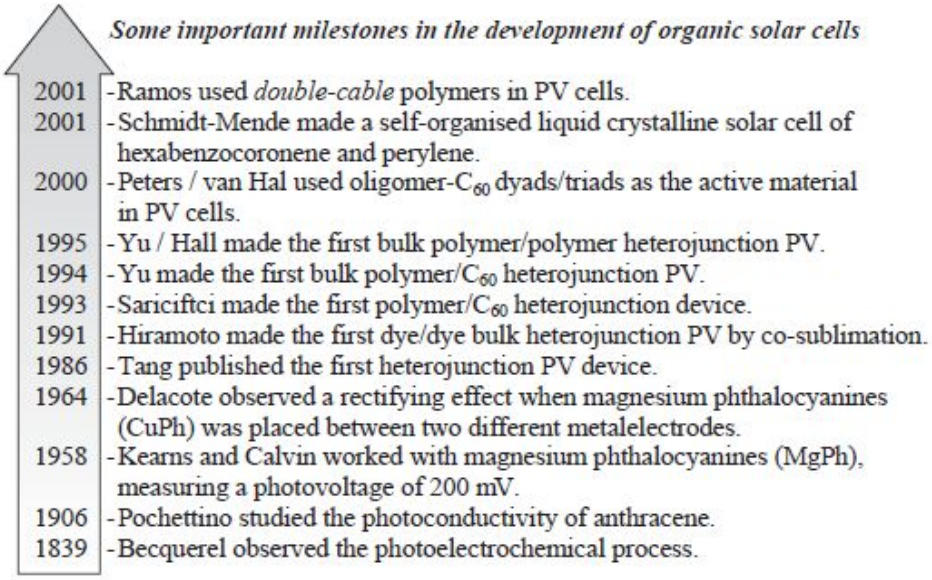

Figure 1.4. Same important milestones in the development of organic solar cells.

1.2.2 Organic Light-Emitting Diodes

After the first EL phenomenon was discovered by Destriau in 1936, EL from organic crystals which is single crystal anthracene was reported in 1963 by Pope.[30] They reported EL from a thick anthracene crystal when a bias of several hundred volts was applied across it. Following this, EL obtained from organic crystals at lower voltages than previous work. But the devices still required high drive voltages due to large crystal thicknesses in the order of tens of micrometers. Due to the high working voltages required to obtain EL from these organic crystal-based devices and the resulting low device efficiencies and lifetimes compared to those obtained from existing inorganic light-emitting devices, research activities were focused on inorganic materials and improving devices with those inorganic materials.

The breakthrough was achieved by Tang and VanSlyke at Eastman Kodak Company in 1987 that made a bilayer structure by thermally evaporating the small molecular weight organic materials.[31] The reported device consisted of a junction formed by vacuum deposition of two thin layers of small molecular weight hole transporting diamine and light emissive-electron transporting tris(8-hydroxyquinoline) aluminum (Alq_3) materials between Indium Tin Oxide (ITO) anode and Mg-Ag cathode. They achieved a novel green-light-emitting organic device with unique characteristics of high EL efficiency, fast response, low drive voltage and simple fabrication procedure initiated worldwide interest in the development of organic light-emitting diodes.

Following the success of fabricating small molecular OLEDs, another significant work concerning the evolution of OLEDs was published in 1990 by Burroughes, where EL was reported from a single-layer of polymer LEDs (PLEDs) by spin coating method.[32] The device consisted of highly fluorescent poly(para-phenylene vinylene) (PPV) polymer as the active material onto a indium tin oxide (ITO) coated glass.

After conductive polymers were discovered by Alan J. Heeger, Alan G. MacDiarmid, and Hideki Shirakawa, these discoveries have led to intense worldwide interest in new materials for incorporation into OLEDs for practical applications: primarily in full-color flat-panel displays and solid state lighting.

1.3 Outline of the Thesis

The introduction chapter covered general knowledge of OPVs and OLEDs. More specific information about the device working principles, materials, fabrication methods, and device structures of OSCs and OLEDs will be discussed in the Chapter 2 and 3, respectively. In Chapter 4, I'll demonstrate that the high performance optoelectronic devices enhanced by surface plasmon effect. Chapter 5 discusses a new approach to white light from a single rod-coil diblock copolymer.

1.4 References

[1] van der Zwaan, Bob & Rabl, Ari 2003, 'Prospects for PV: a learning curve analysis', *Solar Energy*, vol. 74, no. 1, pp. 19-31.

[2] Yu, G., Gao, J., Hummelen, J. C., Wudl, F. & Heeger, A. J. 1995, 'Polymer photovoltaic cells: Enhanced efficiencies via a network of internal donor-acceptor heterojunctions', *Science*, vol. 270, no. 5243, pp. 1789-91.

[3] Brabec, C. J., Sariciftci, N. S. & Hummelen, J. C. 2001, 'Plastic solar cells', *Advanced Funtional Materials*, vol. 11, no. 1, pp. 15-26.

[4] Blom, P. W. M., Mihailetchi, V. D., Koster, L. J. A. & Markov, D. E. 2007, 'Device physics of polymer:Fullerene bulk heterojunction solar cells', *Advanced Materials*, vol. 19, no. 12, pp. 1551-66.

[5] Park, S. H., Roy, A., Beaupré, S., Cho, S., Coates, N., Moon, J. S., Moses, D., Leclerc, M., Lee, K. & Heeger, A. J. 2009, 'Bulk heterojunction solar cells with internal quantum efficiency approaching 100%', *Nature Photonics*, vol. 3, no. 5, pp. 297-303.

[6] Deibe, C., Strobe, T. & Dyakonov, V. 2010, 'Role of the charge transfer state in organic donor-acceptor solar cells', *Advanced Materials*, vol. 22, no. 37, pp. 4097-111.

[7] Chen, H. Y., Hou, J., Zhang, S., Liang, Y., Yang, G., Yang, Y., Yu, L., Wu, Y. & Li, G. 2009, 'Polymer solar cells with enhanced open-circuit voltage and efficiency', *Nature Photonics*, vol. 3, no. 11, pp. 649-53.

[8] Liang, Y., Xu, Z., Xia, J., Tsai, S. T., Wu, Y., Li, G., Ray, C. & Yu, L. 2010, 'For the bright future-bulk heterojunction polymer solar cells with power conversion efficiency of 7.4%', *Advanced Materials*, vol. 22, no. 20, pp. E135-E8.

[9] Zhao, G. J., He, Y. J. & Li, Y. 2010, '6.5% efficiency of polymer solar cells based on poly(3-hexylthiophene) and indene-C60 bisadduct by device optimization', *Advanced Materials*, vol. 22, no. 39, pp. 4355-8.

[10] Jo, J., Kim, S. S., Na, S. I., Yu, B. K. & Kim, D. Y. 2009, 'Time-dependent morphology ewolution by annealing processes on polymer:Fullerene blend solar cells', *Advanced Functional Materials*, vol. 19, no. 6, pp. 866-74.

[11] Moulé, A. J. & Meerholz, K. 2009, 'Morphology control in solution-processed bulk-heterojunction solar cell mixtures', *Advanced Functional Materials*, vol. 19, no. 19, pp. 3028-36.

[12] Hoven, C. V., Dang, X. D., Coffin, R. C., Peet, J., Nguyen, T. Q. & Bazan, G. C. 2010, 'Improved performance of Polymer bulk heterojunction solar cells through The reduction of phase separation via solvent additives', *Advanced Materials*, vol. 22, no. 8, pp. E63-E6.

[13] Kim, J. Y., Kim, S. H., Lee, H. H., Lee, K., Ma, W., Gong, X. & Heeger, A. J. 2006, 'New architecture for high-efficiency polymer photovoltaic cells using solution-based titanium oxide as an optical spacer', *Advanced Materials*, vol. 18, no. 5, pp. 572-6.

[14] Kim, J. Y., Lee, K., Coates, N. E., Moses, D., Nguyen, T. Q., Dante, M. & Heeger, A. J. 2007, 'Efficient tandem polymer solar cells fabricated by all-solution processing', *Science*, vol. 317, no. 5835, pp. 222-5.

[15] 'Organic light emitting diodes for general illumination update; Report', 2002, paper presented to Optoelectronics Industry Development Association (OIDA), august.

[16] Heeger, A. J. 1998, 'Light emission from semiconducting polymers: Light-emitting diodes, light-emitting electrochemical cells, lasers and white light for the future', *Solid State Communications*, vol. 107, no. 11, pp. 673-9.

[17] D'Andrade, B. W. & Forrest, S. R. 2004, 'White organic light-emitting devices for solid-state lighting', *Advanced Materials*, vol. 16, no. 18, pp. 1585-95.

[18] Kido, J., Kimura, M. & Nagai, K. 1995, 'Multilayer white light-emitting organic electroluminescent device', *Science*, vol. 267, no. 5202, pp. 1332-4.

[19] Chen, Z., Ogino, K., Miyata, S., Lu, Y. & Watanabe, T. 2002, 'The pure white light emission from three-layer electroluminescent device', *Journal of Physics D: Applied Physics*, vol. 35, no. 8,

pp. 742-6.

[20] Ho, G. K., Meng, H. F., Lin, S. C., Homg, S. F., Hsu, C. S., Chen, L. C. & Chang, S. M. 2004, 'Efficient white light emission in conjugated polymer homojunctions', *Applied Physics Letters*, vol. 85, no. 20, pp. 4576-8.

[21] Xu, Y., Peng, J., Jiang, J., Xu, W., Yang, W. & Cao, Y. 2005, 'Efficient white-light-emitting diodes based on polymer codoped with two phosphorescent dyes', *Applied Physics Letters*, vol. 87, no. 19, pp. 193502/1-3.

[22] Gong, X., Wang, S., Moses, D., Bazan, G. C. & Heeger, A. J. 2005, 'Multilayer polymer light-emitting diodes: White-light emission with high efficiency', *Advanced Materials*, vol. 17, no. 17, pp. 2053-8.

[23] Becquerel, A.E. 1839, 'Mémoire sur les effets électriques produits sous l'influence des rayons solaires', *Compt. Rend. Acad. Sci*, vol. 9, pp. 561-7.

[24] Destriau, G. 1936, 'Recherches sur les scintillations des sulfures de zinc aux rayons', *Journal de Chemie Physique*, vol. 33, pp. 587-625.

[25] Adams., W.G. & Day., R.E 1876, 'The action of Light on Selenium', *Proceeding of the Royal Society of London*, vol. 25, pp. 113-7.

[26] Pochettino, A. 1906, 'Sul comportamento foto-elettrico dell' antracene', *Acad. Lincei Rend*, vol. 15, pp. 355-68.

[27] Chapin, D. M., Fuller, C. S. & Pearson, G. L. 1954, 'A new silicon p-n junction photocell for converting solar radiation into electrical power', *Journal of Applied Physics*, vol. 25, no. 5, pp. 676-7.

[28] Tang, C. W. 1986, 'Two-layer organic photovoltaic cell', *Applied Physics Letters*, vol. 48, no. 2, pp. 183-5.

[29] Shirakawa, H., Louis, E. J., MacDiarmid, A. G., Chiang, C. K. & Heeger, A. J. 1977,

'Synthesis of electrically conducting organic polymers: Halogen derivatives of polyacetylene, (CH)x', *Journal of the Chemical Society, Chemical Communications*, no. 16, pp. 578-80.

[30] Pope, M., Kallmann, H. P. & Magnante, P. 1963, 'Electroluminescence in organic crystals', *The Journal of Chemical Physics*, vol. 38, no. 8, pp. 2042-3.

[31] Tang, C. W. & Vanslyke, S. A. 1987, 'Organic electroluminescent diodes', *Applied Physics Letters*, vol. 51, no. 12, pp. 913-5.

[32] Burroughes, J. H., Bradley, D. D. C., Brown, A. R., Marks, R. N., Mackay, K., Friend, R. H., Burns, P. L. & Holmes, A. B. 1990, 'Light-emitting diodes based on conjugated polymers', *Nature*, vol. 347, no. 6293, pp. 539-41.

CHAPTER 2
BACKGROUND OF OPVS

This chapter will be covered general information of OPVs on a process of development and device principle, and important parameters. In general, OPVs have been greatly achieved according to the development of the device structure. For the device, I'll introduce the critical parameters characterizing the device performance and operating principles more detail.

2.1 Types of Junctions for OPV Cells

2.1.1 Single Layer OPV Cells

The single layer OSCs are the simplest form among various organic solar cell structures which are comprised of a transparent electrode/organic light-absorbing material/metal electrode as shown in **Figure 2.1a**. Typically, the solar cell is sandwiched between an ITO glass as a bottom electrode, that is, the hole-collecting anode, and thermally evaporated metals as a top electrode such as Al, Ag, and Au, that is, the electron-collecting cathode.

The potential of work function between two different electrodes sets up an electric field across the organic layer. When light is absorbed in the organic layer, electrons are promoted from the highest occupied molecular orbital (HOMO) to the lowest unoccupied molecular orbital (LUMO) forming excitons. The potential created by the asymmetric work functions helps to separate the exciton pairs, where electrons must reach one electrode while the holes must reach the other electrode.

After Kearns reported the photovoltaic effect with magnesium phthalocyanines (CuPh),[1] Weinberger used polyacetylene as an organic layer, which had an open circuit voltage (V_{oc}) of 0.3V and power conversion efficiency (PCE) of 0.3% in 1982.[2] Karg fabricated an ITO/PPV/Al cell, showing V_{oc} of 1V and PCE of 0.1% under white light illumination.[3]

However, single layer organic solar cells have several problems, for example, low quantum efficiency due to the intrinsically low mobility of charges and low PCE attributed to the exciton formation, which are strongly bound dipole charges of photoexcited semiconducting organics. To solve these problems, the bilayer cell was developed by inserting an acceptor layer between a donor organic material and a cathode for the more efficient dissociation.

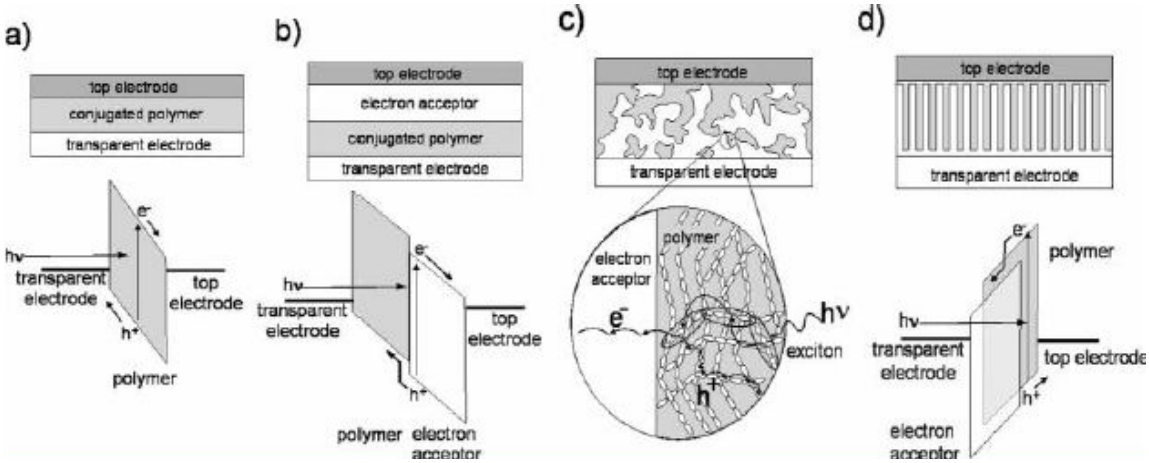

Figure 2.1. Four device architectures of conjugated polymer-based photovoltaic cells (a) single-layer PV cell (b) bilayer PV cell (c) disordered bulk heterojunction (d) ordered bulk heterojunction.

2.1.2 Bilayer OPV Cells

The bilayer OPV cell structure includes an additional electron transporting layer between the conductive electrodes as depicted in **Figure 2.1b**. Two different layers have differences in electron affinity and ionization energy, energy level offsets at heterjunctions are shown to be essential to the operation of device because of the fundamental nature of the photogeneration process. One key improvement to the structure of OPV cells made by Tang in 1985 when he discovered that, by making two-layer PV cells with organic semiconductors that have offset energy bands, the external quantum efficiency (EQE) improved to 15% at the maximum absorption wavelength. This increase resulted from improving exciton dissociation efficiency by adding electron transporting material that forms an offset energy band with hole transporting material.

In 1993, first bilayer technique was applied to a conjugated polymer PV cell by evaporating C_{60} as an electron transporting material on top of a spin-cast poly[2-methoxy-5-(2'-ethyl-hexyloxy)-l,4-phenylene vinylene] (MEH-PPV) hole transporting material by Sariciftci.[4] In this OPV cell, the obtained PCE was 0.04% under monochromatic incident light, and showed only a slight improvement over pure polymer films. Halls optimized the thickness of MEH-PPV and C_{60} layer and obtained 9% EQE.[5]

In bilayer OPV cells, the diffusion length of excitons in organic electronic materials is typically on the order of 10-20nm. For more efficient diffusion of exciton, the organic layer is needed in the same range with the diffusion length. Because the exciton diffusion length in a conjugated polymer is typically less than the absorption length of the material, the EQE of a bilayer device made with a conjugated polymer and another semiconductor is ultimately limited by the number of photons that can be absorbed within an exciton diffusion length of the interface.

2.1.3 Bulk Heterojunction OPV Cells

Bulk heterojunction is a blend of the donor and acceptor materials in a bulk which exhibits phase separation in a 10-20nm in a nanoscale interpenetrating network system. (**Figure 2.1c, d**) In the bilayer structure, the donor and acceptor phases are completely separated from each other, while both phases of the bulk heterojunction are intimately intermixed. From this point, the bulk heterojunction system has increased the interfacial area than bilayer and resulted in significantly improved efficiency in the cells.

Yu investigated a phase-separated polymer blend composite made of MEH-PPV as a donor and cyano-PPV (CN-PPV) as an acceptor.[6] The photoluminescence from each of the polymers was quenched, which indicates that the rapid and efficient separation of photogenerated electron-hole pairs within the film reaches an interface with the other polymer and dissociated before recombining. This cell gave 0.9% PCE, which is 20times larger than that of made bilayer with same materials.

In 1995, Yu founded that, by the blending of conjugated polymer with a solublized form of C_{60}, called (6,6)-phenyl C_{61}-butyric acid methyl ester (PCBM), the better photoluminescence quenching and carrier transport could be achieved, resulting in 2.9% PCE as shown in **Figure 2.2**.[7]

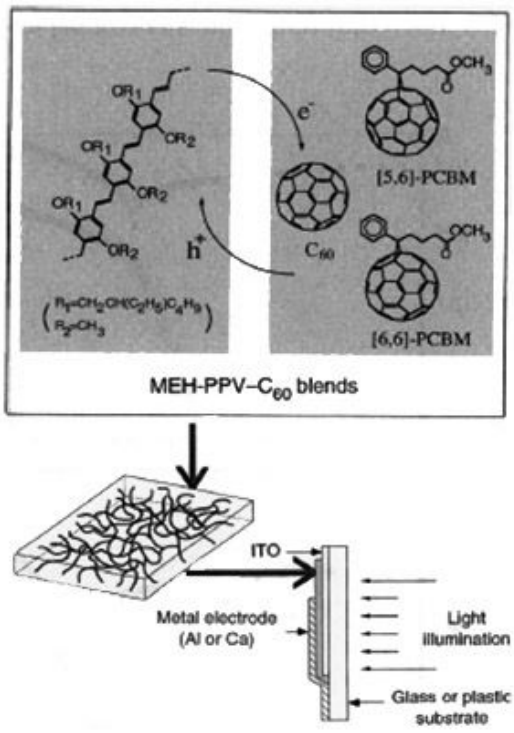

Figure 2.2. Schematic diagram of the photoinduced from charge transfer process in MEH-PPV : C_{60} D-A blends.

The next significant improvement in OPV fields was by using poly(3-hexylthiophene) (P3HT) as a hole transporting polymer. Padinger switched the conjugated polymer from PPV derivatives to P3HT and it achieved a further increase with 3.5% PCE under white light illumination.[8]

In 1995, Li fabricated a blend OPV cell using P3HT and PCBM of PCE of 4.4%.[9] This significant improvement in efficiency is attributed to controlling the active layer growth rate resulting in an increased hole mobility and balanced charge transport. By solvent annealing, P3HT and PCBM formed an interdigitated blend film where P3HT forms crystalline morphology and PCBM aggregates are embedded and this phase separated morphology enhanced mobility of the conjugated polymer.

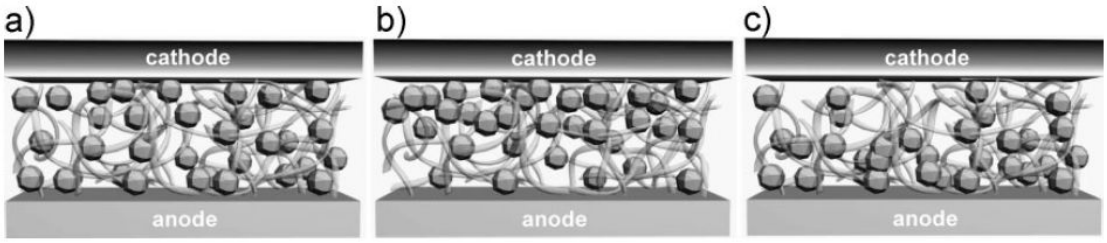

Figure 2.3. Schematic illustrations of vertical component distributions in the cross-sectional active layer of the composite film induced depending on the solvent annealing conditions a) a homogeneous distribution, b) a PCBM-rich, and c) a PCBM-poor distribution near the top electrode.

For the hybrid solar cells, inorganic nanoparticles instead of PCBM or C_{60} were blended with conjugated polymer such as quantum dot, metal oxide nanoparticles. Organic materials usually are inexpensive, easily processable, and their functionality can be tailored by molecular design and synthesis, while inorganic materials have tenability of photophsical properties.

2.2 Device Physics of the OPVs

2.2.1 Basic Process in OPVs

The process of conversion of light into electricity of OPVs can be schematically described by the following steps:[10] (**Figure 2.4**)

Step1. Light absorption

Step2. Exciton dissociation

Step3. Charge transfer

Step4. Charge collection

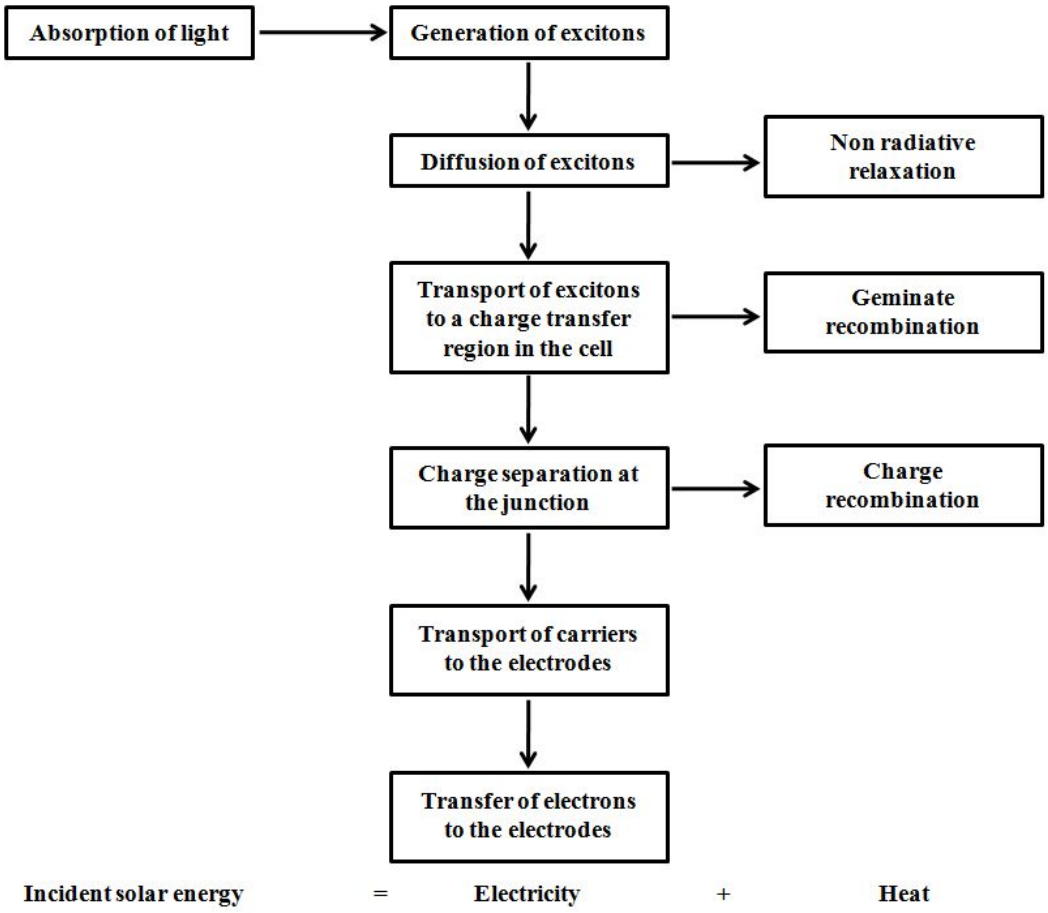

Figure 2.4. Conversion steps and loss mechanism of light power into electric power.

To create a working OPV cells, photoactive materials are sandwiched between two electrodes. Absorption of a photon leading to the formation of an excited state, the bound electron-hole pair creation, exciton diffusion to a region where exciton dissociation, that is, charge separation occurs, and charge transport within the organic semiconductor to the respective electrodes.

2.2.1.1 Light Absorption

The first step is light absorption leading to formation of exciton. When sunlight is absorbed in photoactive materials, an electron is promoted from HOMO to LUMO forming an exciton. For an efficient collection of photons, the absorption spectrum of the photoactive organic layer should match the solar emission spectrum and the layer should be sufficiently thick to absorb all incident light. In case of organic devices, only a small portion of the incident light is absorbed since the bandgap is too high. A bandgap of 1.1eV is required to absorb 77% of the solar radiation on earth whereas the majority of semiconducting polymers have bandgap higher than 2.0eV, limiting the possible absorption to about 30%.

A better overlap with the solar emission spectrum is obtained by lowering the band gap of the organic material, but this will ultimately have some bearing on V_{oc}. Increasing the layer thickness is advantageous for light absorption, but burdens the charge transport.

2.2.1.2 Exciton Dissociation

Charge creation is one of the main steps in photovoltaic devices in the conversion of solar light into electrical energy. In most organic solar cells, charges are created by photoinduced electron transfer. In this reaction an electron is transferred from an electron donor (D), a p-type semiconductor, to an electron acceptor (A), an n-type semiconductor, with the aid of an absorbed photon (hv). In the photoinduced electron transfer reaction the first step is excition of the donor (D*) or the acceptor (A*), followed by creation of the charge-separated state consisting of the radical cation of the donor ($D^{\bullet+}$) and the radical anion of the acceptor ($A^{\bullet-}$).

$$D + A + h\nu \rightarrow D^* + A \text{ (or } D + A^*) \rightarrow D^{\bullet+} + A^{\bullet-}$$

Ideally, all photoexcited excitons should reach a dissociation site. Since such a site may be at the other end of the semiconductor, their diffusion length should be at least equal to the layer thickness for sufficient absorption, otherwise they recombine and photons are wasted. Exciton diffusion lengths in organic semiconductors are usually around 10-20 nm.

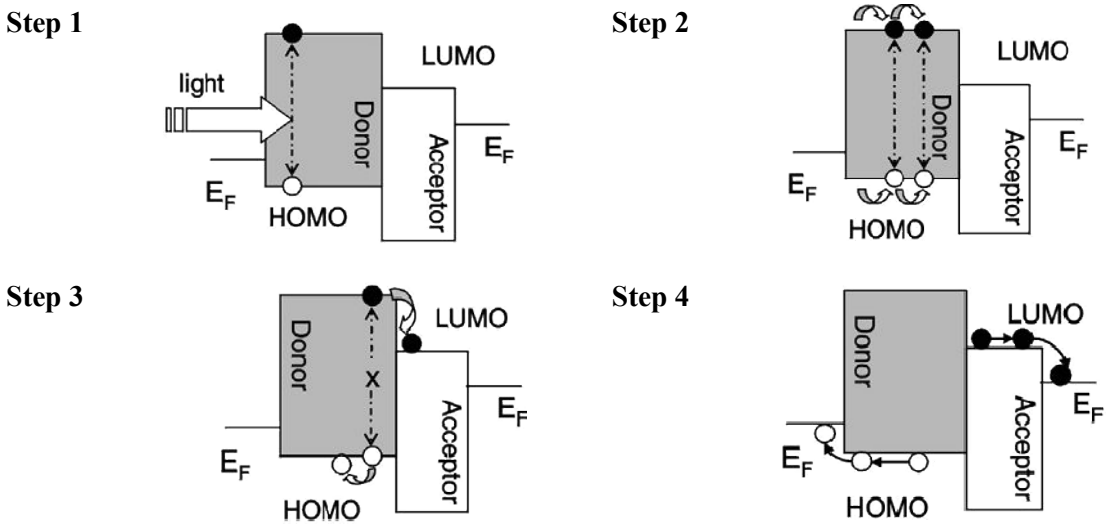

Figure 2.5. Principle of solar cell operation.

2.2.1.3 Charge Transfer

The energy of the absorbed photon is used for generation of the charge separated state and is affected by recombination process during the journey to the electrodes. The charge carriers need two driving forces to reach the electrodes; a gradient in the chemical potentials of electrons and holes and the concentration gradients of the respective charges, which lead to a diffusion current. When the charge separated state is stabilized, the photogenerated charges can migrate to one of the electrodes.

2.2.1.4 Charge Collection

The last step is charge collection that charge carriers are extracted from the device through two selective contacts. The collection of charge carriers at the electrodes is regularly accomplished by a transparent conductive oxide (TCO) such as ITO or FTO on one side and a metal contact on the other side with accompanied with ohmic contact between the electrodes and the molecular layer. Well-matched work function of two electrodes is one of the important factors in OPVs.

2.2.2 Characteristics of OPVs

2.2.2.1 Efficiency

The photovoltaic power conversion efficiency of a solar cell is determined by the following formula:

$$\eta_e = \frac{V_{oc} * I_{sc} * FF}{P_{in}}$$

These four quantities: V_{oc}, I_{sc}, FF and η_e are the key parameters of a solar cell under illumination conditions. V_{oc} is the open circuit voltage, I_{sc} is the short circuit current, FF is the fill factor, and P_{in} is the incident light power density. The Standard Test Condition (STC) for solar cells is the Air Mass 1.5 spectrum, an incident power density of 1000 W m^{-2}. (**Figure 2.6**)

The open circuit voltage is the difference of electric potential between two terminals of a device when there is no external load connected. Generally, in case of metal-insulator-metal device is determined by the work function difference of two metal contacts,[11] while the maximum available voltage is determined by the difference of the quasi Fermi levels of the two semiconductors in *p-n* junction. For organic solar cells, the open circuit voltage is linearly dependent on the HOMO level of the donor and LUMO level of the acceptor.[12] For the ideal diode,

$$V_{oc} = \frac{kT}{q} \ln\left(\frac{J_{sc}}{J_o} + 1\right)$$

where, J_o is a constant, k is Boltzmann's constant and T is temperature.

The short circuit current is the current through the solar cells when the voltage across the device is zero, which is determined by the product of the photoinduced charge carrier density and the charge carrier mobility within the organic semiconductors.

$$I_{sc} = ne\mu E$$

where, n is the charge carrier density, e is the elementary charge, μ is the mobility, and E is the electric field.

Fill factor is determined by charge carriers reaching the electrodes, when the built-in field is reaching toward the open circuit voltage. Hence, the mobility and series resistances influence the fill factor. It is defined as the ratio of the actual maximum obtainable power to the theoretical power.

$$FF = \frac{I_{mpp} * V_{mpp}}{I_{sc} * V_{oc}}$$

where, I_{mpp} and V_{mpp} is the maximum power output of the current and voltage.

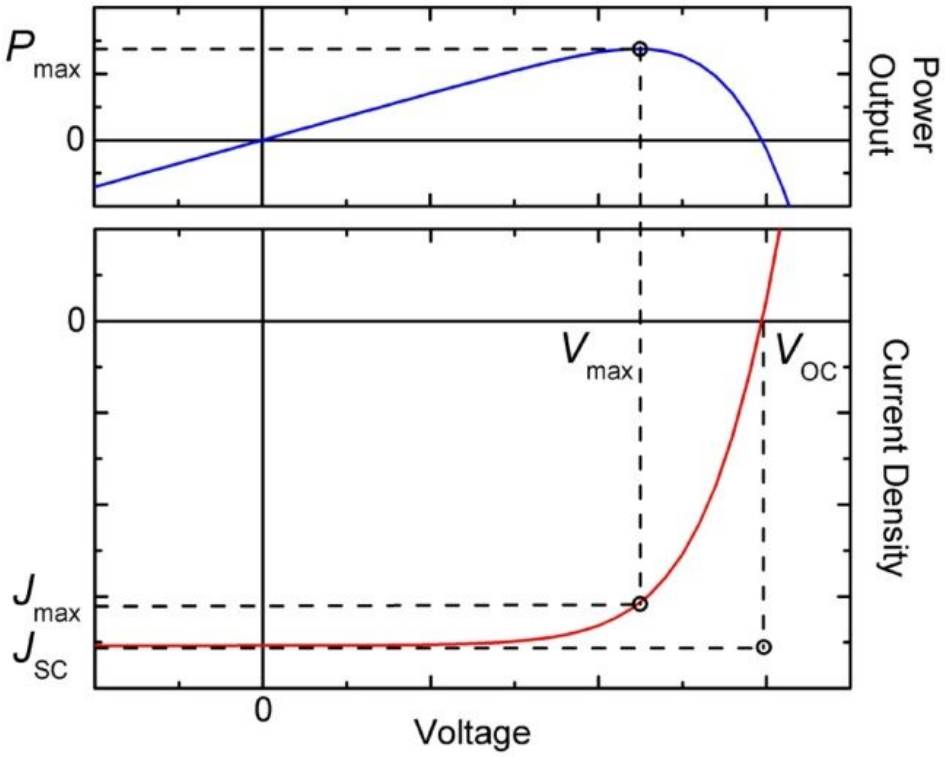

Figure 2.6. The current-voltage characteristic of a solar cell and corresponding electrical power density output.

2.2.2.2 Quantum Efficiency

Quantum Efficiency (QE) is the ratio of the number of charge carriers collected to the number of photons of a given energy shining on the solar cells. Photon energy varies with the wavelength of photon, and QE depends on the different wavelengths of light.

In solar cells, two types of QE are considered, external quantum efficiency (EQE) and internal quantum efficiency (IQE) as shown in **Figure 2.7**. EQE is the ratio of the number of photogenerated electrons collected under short circuit conditions to the number of incident photons.[13]

$$EQE = \eta_A * \eta_{diff} * \eta_{diss} * \eta_{tr} * \eta_{cc}$$

where, η_A is the photon absorption yield which is determined by the optical absorption coefficient of the photoactive materials. η_{diff} is the exciton diffusion yield, which represents the

ability of exciton to diffuse through the polymer without recombination. The parameter η_{diss} is the exciton dissociation yield which is the probability that the hole and electron will be separated by the internal electric field at a heterojunction. η_{tr} value is the charge carrier transport yield and η_{cc} is the charge collection yield which represents the ability of the charges to be transferred from the photoactive layer to the electrodes.

IQE is the ratio of the number of charge carriers collected by the solar cell to the number of photons of a given energy that shine on the solar cell from outside and is absorbed by the cell without reflection and transmittance. Poor IQE value indicates that many electrons are recombination. Poor EQE can be either a reflection of poor internal efficiency or can mean that large amounts of the light reaching the cell are unavailable for use because it is being reflected away by the cell or allowed to pass through it.

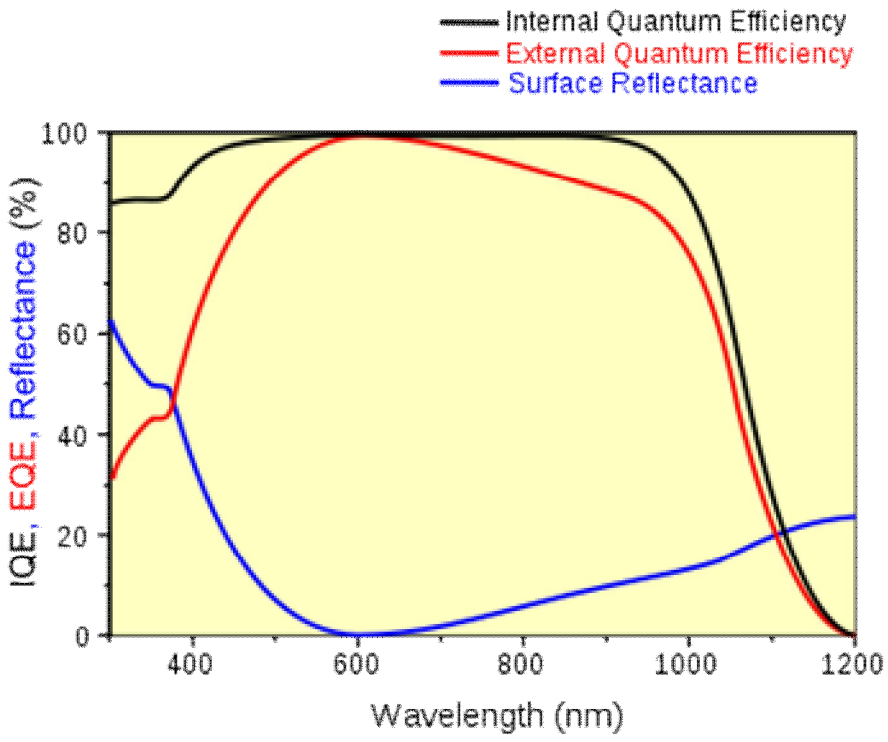

Figure 2.7. IQE, EQE, and reflectance with wavelength.

2.3 Materials and Methods

2.3.1 General Materials

General Materials for OSCs is the conjugated polymer having a delocalized π-electron system which can absorb light, create photogenerated charge carrier, and transport charges.[14]

Research on organic solar cells generally focuses either on solution processable organic semiconducting molecules/polymers or on vacuum-deposited small-molecular materials. As an example, phthalocyanine is a representative of the p-type, hole conducting material that works as electron donor. Perylene and its derivatives show an n-type, electron conducting behavior and serve as electron acceptor materials.

In addition, for hole conducting donor type polymers, poly[2-methoxy-5-(3,7-dimethyloctyloxy)]-1,4-phenylenevinylene (MDMO-PPV), poly(3-hexylthiophene) (P3HT) are mainly used together with electron-conducting acceptor polymers like poly-[2-methoxy-5-(2'-ethylhexyloxy)-1,4-(1-cyanovinylene)-phenylene (CN-MEH-PPV), and poly(9,9'-dioctylfluoreneco-benzothiadiazole) (F8TB), and a soluble derivative of C_{60}, namely PCBM. (**Figure 2.8**)

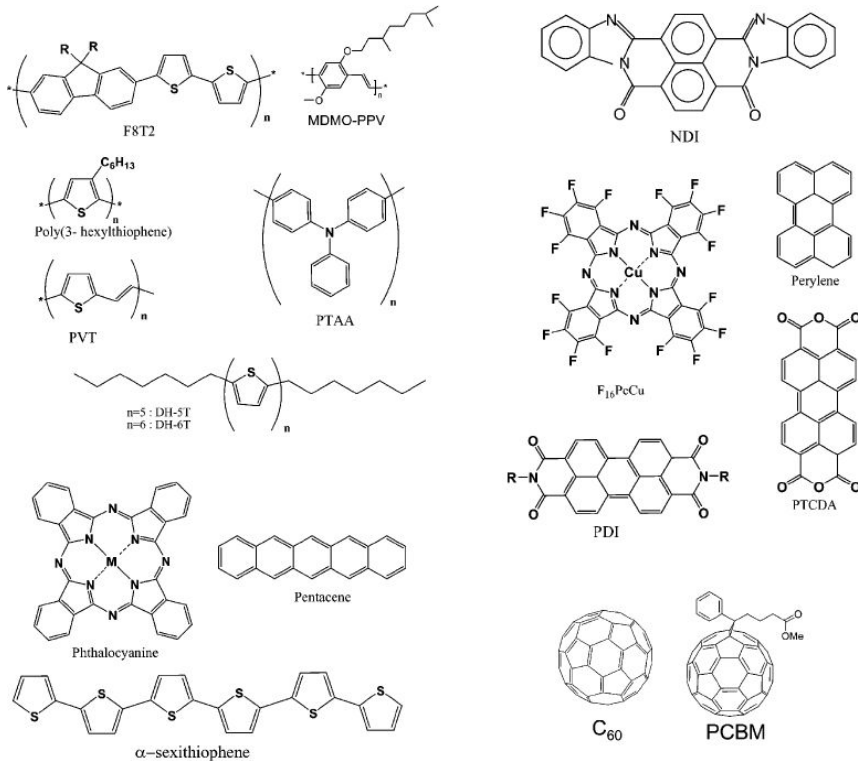

Figure 2.8. Examples of organic semiconductors used in organic solar cells.

2.3.2. Preparation Techniques

Vacuum evaporation and solution processing techniques are commonly used for preparation of thin film in the production of OSCs. For materials for evaporation, thermal stability is required due to decomposition of polymer under excessive heat. For that reason, evaporation method is used for small molecules which have more thermally stable than polymers. Most of polymer based photovoltaic elements are solution processed at low temperatures. The printing/coating techniques are used to deposit conjugated polymers, for example, (a) spin coating, (b) doctor blading, (c) screen printing, and (d) inkjet printing, as presented in **Figure 2.9**.[14]

(a)

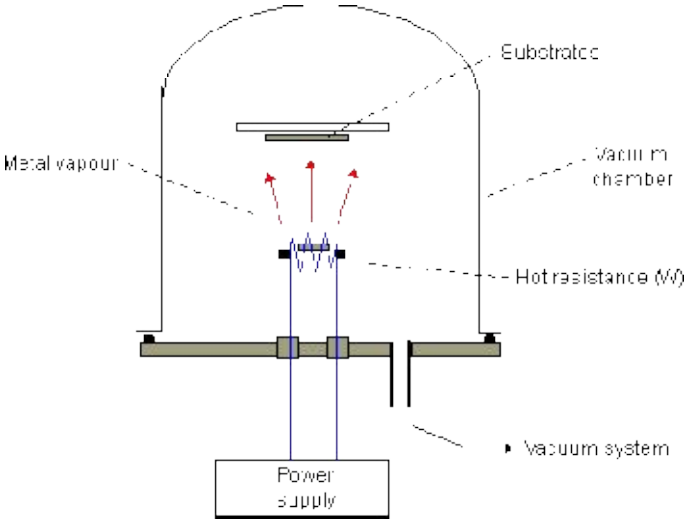

(b)

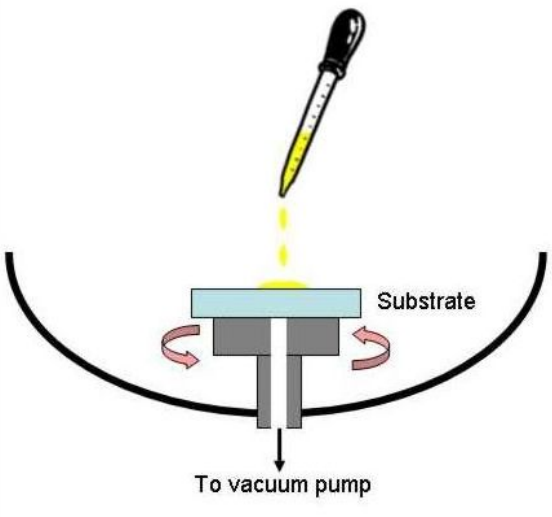

Figure 2.9. (a) vacuum evaporation (b) spin-coating.

2.4. References

[1] Keaens, D. & Calvin, M. 1958, 'Photovoltaic effect and photoconductivity in laminated organic systems', *The Journal of Chemical Physics*, vol. 29, no. 4, pp. 950-1.

[2] Weinberger, B. R., Akhtar, M. & Gau, S. C. 1982, 'Polyacetylene photovoltaic devices', *Synthetic Metals*, vol. 4, no. 3, pp. 187-97.

[3] Karg, S., Riess, W., Dyakonov, V. & Schwoerer, M. 1993, 'Electrical and optical characterization of poly(phenylene-vinylene) light emitting diodes', *Synthetic Metals*, vol. 54, no. 1-3, pp. 427-33.

[4] Sariciftci, N. S., Braun, D., Zhang, C., Srdanov, V. I., Heeger, A. J., Stucky, G. & Wudl, F. 1993, 'Semiconducting polymer-buckminsterfullerene heterojunctions: Diodes, photodiodes, and photovoltaic cells', *Applied Physics Letters*, vol. 62, no. 6, pp. 585-7.

[5] Halls, J. J. M., Pichler, K., Friend, R. H., Moratti, S. C. & Holmes, A. B. 1996, 'Exciton diffusion and dissociation in a poly(p-phenylenevinylene)/C60 heterojunction photovoltaic cell', *Applied Physics Letters*, vol. 68, no. 22, pp. 3120-2.

[6] Yu, G. & Heeger, A. J. 1995, 'Charge separation and photovoltaic conversion in polymer composites with internal donor/acceptor heterojunctions', *Journal of Applied Physics*, vol. 78, no. 7, pp. 4510-5.

[7] Yu, G., Gao, J., Hummelen, J. C., Wudl, F. & Heeger, A. J. 1995, 'Polymer photovoltaic cells: Enhanced efficiencies via a network of internal donor-acceptor heterojunctions', *Science*, vol. 270, no. 5243, pp. 1789-91.

[8] Padinger, F., Rittberger, R. S. & Sariciftci, N. S. 2003, 'Effects of postproduction treatment on plastic solar cells', *Advanced Functional Materials*, vol. 13, no. 1, pp. 85-8.

[9] Li, G., Shrotriya, V., Huang, J., Yao, Y., Moriarty, T., Emery, K. & Yang, Y. 2005, 'High-efficiency solution processable polymer photovoltaic cells by self-organization of polymer blends', *Nature Materials*, vol. 4, no. 11, pp. 864-8.

[10] Nunzi, Jean-Michel 2002, 'Organic photovoltaic materials and devices', *Comptes Rendus Physique*, vol. 3, no. 4, pp. 523-42.

[11] Parker, I. D. 1994, 'Carrier tunneling and device characteristics in polymer light-emitting diodes', *Journal of Applied Physics*, vol. 75, no. 3, pp. 1656-66.

[12] Brabec, C. J., Cravino, A., Meissner, D., Serdar Sariciftci, N., Fromherz, T., Rispens, M. T., Sanchez, L. & Hummelen, J. C. 2001, 'Origin of the open circuit voltage of plastic solar cells', *Advanced Funtional Materials*, vol. 11, no. 5, pp. 374-80.

[13] Moliton, A. & Nunzi, J. M. 2006, 'How to model the behaviour of organic photovoltaic cells', *Polymer International*, vol. 55, no. 6, pp. 583-600.

[14] Günes, S., Neugebauer, H. & Sariciftci, N. S. 2007, 'Conjugated polymer-based organic solar cells', *Chemical Reviews*, vol. 107, no. 4, pp. 1324-38.

CHAPTER 3
BACKGROUND OF OLEDS

This chapter will be covered general information of OLEDs on simple device structure, working principles, and main factors for device characteristics.

3.1 Basic Structure of OLEDs

Electroluminescence is a process which involves non-thermal generation of light from a material under electric field. After EL was first discovered for inorganic materials by Destriau,[1] OLEDs have received much attention over many years due to their potential for applications in full color displays and solid state lighting.

The first OLED was reported by Tang and Van Slyke in 1987 at Eastman Kodak.[2] The structure of a simple bilayer OLED consists of a hole transport layer (HTL) and electron transport layer (ETL) sandwiched between an anode and cathode.

3.1.1 Single Layer OLEDs

The simplest OLED devices is consisting of one active layer with two injecting contact as shown in **Figure 3.1a**. For more efficient charge injection, the work function of the cathode metal is usually low to facilitate efficient electron injection into the active material while the work function of the semi transparent anode is preferable high. Holes injected from the anode are transported toward the cathode by the high electric field and recombine with electrons injected from the cathode. Parker has made a conclusion that carrier injection in such devices is governed principally by the tunnel barriers, since most organic materials used in thin-film LEDs do not transport both carrier types with comparable mobility.[3,4] Generally, single layer devices give very poor efficiency and brightness.

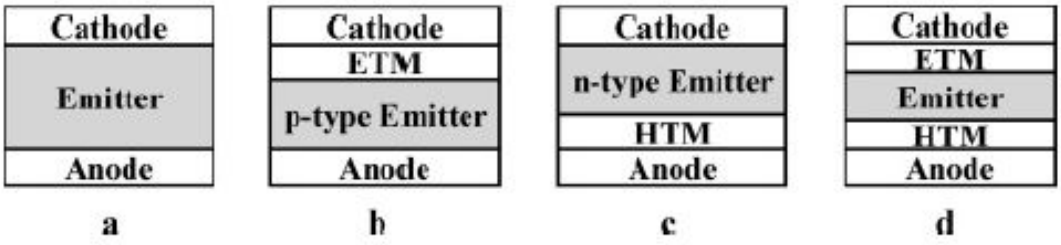

Figure 3.1. (a) single layer device structure, (b)-(d) multilayer device structure.

3.1.2 Multilayer OLEDs

The use of two or more different materials to perform the required functions of efficient light emission and good electron injection and hole injection and transport properties in an OLED has resulted in orders of magnitude improvement in device performance. (**Figure 3.1b-d**)

The introduction of one or more layers of charge transport materials in addition to the emitter layer provides a powerful means to controlling charge injection, transport, and recombination in OLEDs. The presence of an ETM layer in the two layer OLED configuration based on a p-type emitter not only lowers the barrier for electron injection but also serves to block holes since the ionization potential (IP) of ETMs are generally large. Since hole mobility is orders of magnitude larger than electron mobility in most emissive organic semiconductors, existence of an ETM layer can dramatically reduce the hole current and the greater electron mobility than hole mobility in the ETM. Similarly an HTM layer in combination with an n-type emitter, such as aluminum quinolate (Alq3)[5] or polyquinoline[6], can significantly improve OLED performance, in this case, the HTM facilitates hole injection and blocks electrons.

3.2 Device Physics of OLDEs

3.2.1 Basic Process of OLDEs

The working mechanism of OLEDs can be described in three different stages as follows:[7]

Step1. Carrier injection

Step2. Carrier transport

Step3. Carrier recombination and emission (**Figure 3.2**)

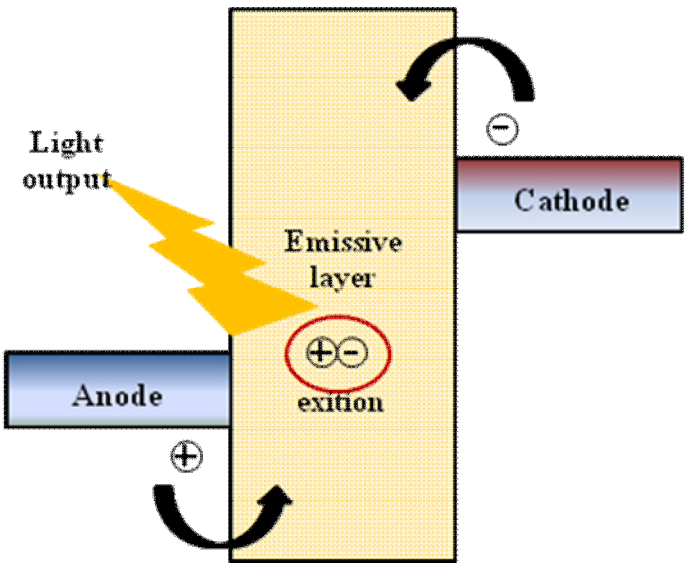

Figure 3.2. Principle of OLEDs.

This first stage of carrier injection involves the injection of carriers from the electrodes into the organic layers in the presence of an applied electric field. Carrier injection and transportation properties in OLEDs are determined by hopping of charge carriers between localized states in the organic layers and from delocalized states in the metal to localized states in the organic layer.[8] When a forward bias is applied, holes are injected from the positively biased anode into the HTL and electrons are injected from the negatively biased metal cathode into the ETL.

If two molecules are separated by a potential barrier, a carrier on one can move to the other either by tunneling through the barrier or by moving over the barrier via an activated state, called hopping. The actual transit rate from one site to another depends on their energy difference and on the distance between them. The energy states involved in the hopping transport of holes and electrons form narrow bands around the HOMO and LUMO levels.

Taking the traps within the organics into consideration, charge transport through the organic layers can be divided into four different regimes: ohmic, space-charge limited, trap-charge limited and trap-filled space-charge limited.[9]

After carrier injection and transport, both electrons and holes can recombine to form various excited states such as singlet and triplet exitons, where parallel spin pairs recombine to form triplet excitons and anti-parallel spin pairs recombine to form singlet excitons.[10] (**Figure 3.3**)

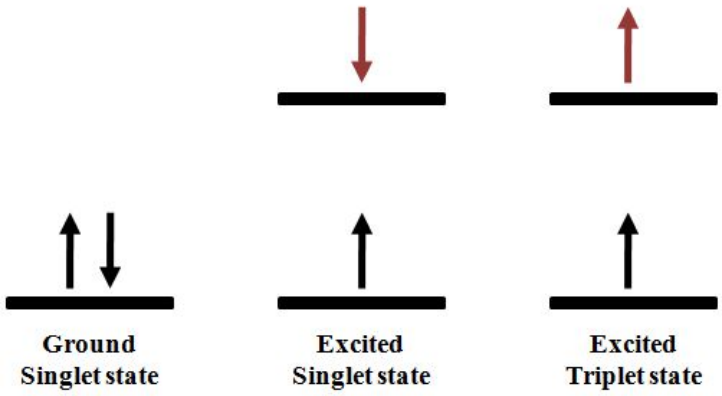

Figure 3.3. Various excited states of excitons.

Statistically, the carrier recombination creates singlet and triplet excitons at a ratio of 1:3. In fluorescent OLEDs, singlet excitons decay radiatively and in phosphorescent OLEDs, both singlets and triplets contribute to photon emission. The HOMO and LUMO levels of the organic materials used in the device help determine in which layer the carriers recombine and photon emission occurs.

3.2.2 Performance Parameters

In OLED, there are various parameters such as external quantum efficiency, luminance, luminance efficiency, radiance, radiance Efficiency and lifetime which indicate the performance characteristics of a particular device. In this section, EQE and luminance efficiency will be described in detail as they are two important parameters.

3.2.2.1 Quantum Efficiency

The active region of an ideal OLED emits one photon for every electron injected. Each charge quantum-particle (electron) produces one light quantum-particle (photon).

The internal quantum efficiency is defined as

$$\eta_{\text{int}} = \frac{\text{number of photons emitted from active region per second}}{\text{number of electrons injected into LED per second}} = \frac{P_{\text{int}}/(h\nu)}{I/e}$$

where P_{int} is the optical power emitted from the active region and I is the injection current.

Photons emitted by the active material should escape from the device. In an ideal ideal, all photons are emitted into free space. It is represented

$$\eta_{\text{extraction}} = \frac{\text{number of photons emitted into free space per second}}{\text{number of photons emitted from active region per second}} = \frac{P/(h\nu)}{P_{\text{int}}/(h\nu)}$$

where P is the optical power emitted into free space. In extraction, it has several loss mechanisms such as reabsorbing in the substrate, light trapping, and internal reflection.

The external quantum efficiency is defined as

$$\eta_{\text{ext}} = \frac{\text{number of photons emitted into free space per second}}{\text{number of electrons injected into LED per second}} = \frac{P/(h\nu)}{I/e} = \eta_{\text{int}} * \eta_{\text{extraction}}$$

The external quantum efficiency gives the ratio of the number of useful light particles to the number of injected charge particles.

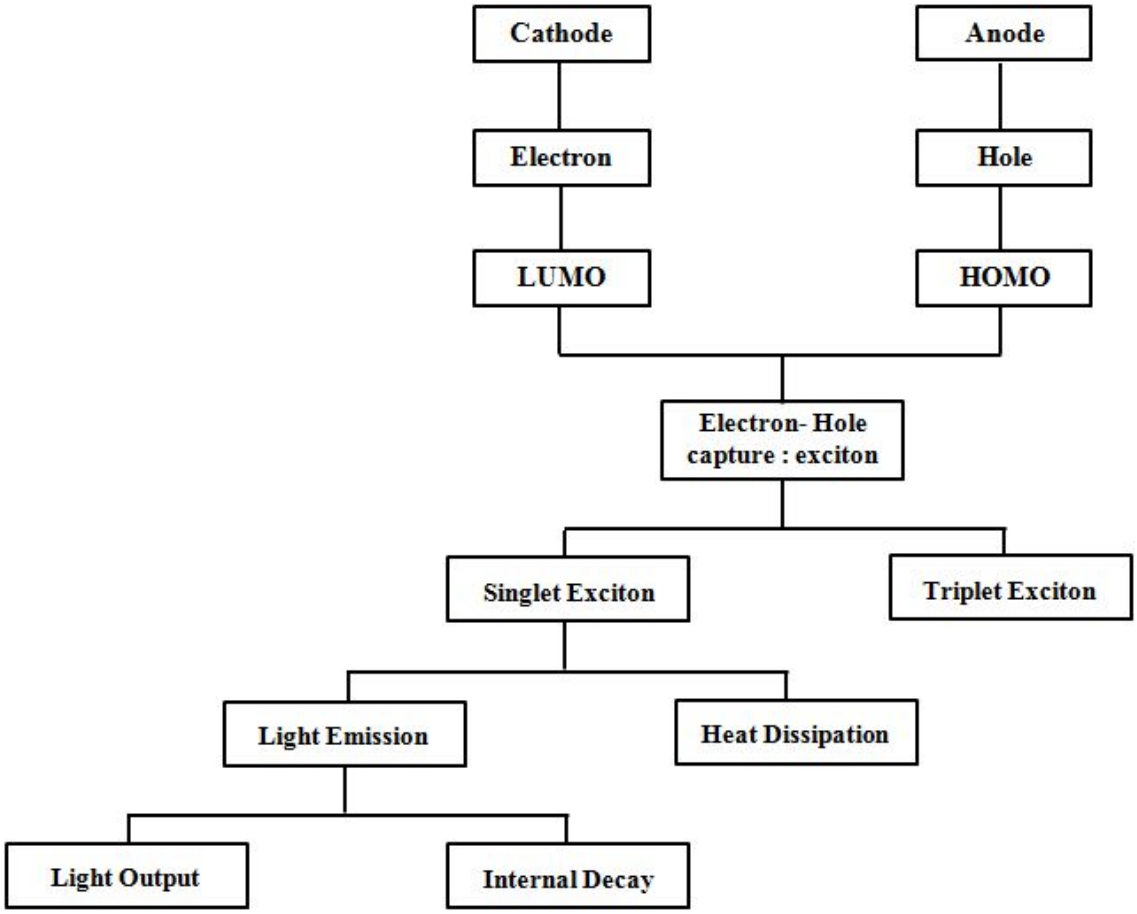

Figure 3.4. Scheme of EL process.

3.2.2.2 Luminance Efficiency

The luminance efficiency or the luminance current efficiency (cd/A) is the ratio of the luminance (L, cd/m^2) of the light emitted to the input current density (J, A/m^2). The luminance current efficiency is useful for gauging the influence of current on the device performance.

3.2.2.3 Color Quality

There are two critical parameters which define the color quality of a light source, the color rendering index (CRI)[11] and Commission Internationale d'Eclairage (CIE) chromaticity.[12] For general illumination a light source should have good color rendering performance equivalent to that of a black body source at 3000-6000 K, high-energy efficiency and Commission Internationale d'Eclairage (CIE-1931) chromaticity coordinates (x, y) close to the equal energy white (EEW) (0.33, 0.33). CRI is a numerical measurement of how true colors look when illuminated with the light source. It is measured in 0-100 scales, with 100 representing true color reproduction. The color of light is expressed by the CIE colorimetry system. (**Figure 3.5**) Any color can be expressed by the chromaticity coordinates x and y on the CIE chromaticity diagram. The boundaries of this horseshoe-shaped diagram are the plots of monochromatic light, called spectrum loci, and all the colors in the visible spectrum fall within or on the boundary of this diagram.

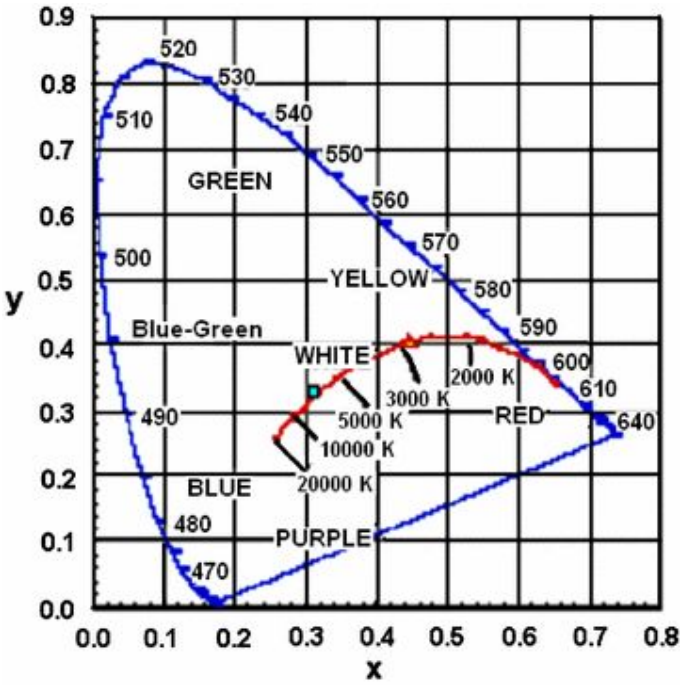

Figure 3.5. CIE (x, y) chromaticity diagram.

3.3 White OLEDs

The history of OLEDs that emit white light started some 15 years ago when Kido and coworkers reported that they had succeeded in fabricating OLEDs generating light that contained wavelengths across the entire visible part of the spectrum.[13] To date, researchers throughout the world in both industry and academia are developing these WOLEDs for the next generation of solid-state light sources and backlighting for flat-panel displays.

As a source of white light, an ideal WOLED should emit a continuous spectrum covering the entire visible range. White light can be obtained an appropriate combination of the three primary colors, red, blue and green, or any two complementary colors such as cyan and red.

In this section, I'll briefly cover how to realize to emit white light and the related physics.

3.3.1 Approaches to White Light Generation

3.3.1.1 Multilayer WOLEDs

The first multilayer WOLED of multilayer type was reported in 1995 by Kido based on vacuum deposited small molecules.

Generally, a high-energy emitter and a relatively low-energy emitter can be combined to obtain white light emission. In multi-layer electroluminescent devices consisting of red, blue and green emitting layers, the spatial location of recombination zones are controlled by matching the HOMO and LUMO levels of each layer or even by the application of hole or electron blocking layers in the device. (**Figure 3.6a**) However, one of the drawbacks of this scheme is that the emission spectrum usually changes as the voltage applied to the device is increased because the resulting increase in the internal electric field has a different effect on the kinetics of electrons and holes.[14]

(a) (b)

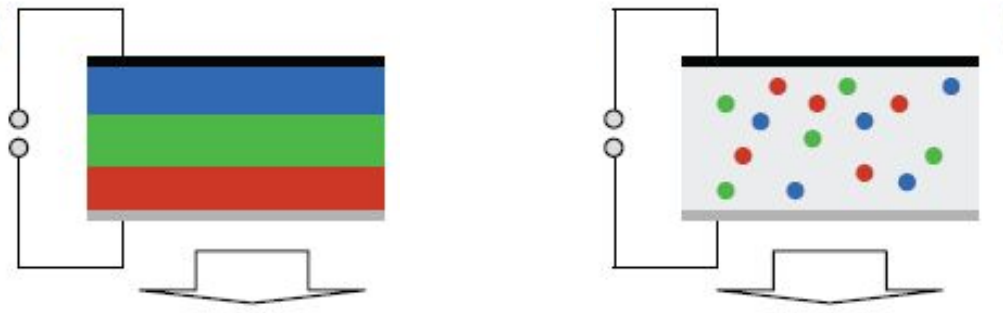

Figure 3.6. The approaches to generate white lightfrom OLEDs include: (a) using a single device stack with several layers emitting in different regions of the spectrum on top of each other, (b) blending lumiphores emitting at different colors into a single layer.

3.3.1.2 WOLEDs by Blending

Possibly the most straightforward way to combine the different lumiphores required to generate white light, is to blend them. In this approach, the emitting layers are doped with photoluminescent dyes to precisely tune the color of the light emitted from each of the layers. (**Figure 3.6b**) For color tuning using dye doping, energy transfer from the host to the dopants results in light emission that is a combination of emission from both the host and the dopants. By altering the dopants or changing the concentrations of the dopants in the host layer, the color of the light emitted from the device can be closely controlled.

Doping the matrix material with one or several lumiphores risks that the blend phase-separates over time which will result in film inhomogeneities, shifts in the color of the emitted light, and a local increase in current density. Due to their generally lower miscibility, polymeric materials are particular prone to this effect.

However, blending approaches are generally considered to offer simpler device fabrication than the multilayer approaches. If all components required to generate white light are mixed into one material, one can fabricate a WOLED with a single active layer that is sandwiched between two electrodes. This reduces the number of processing steps for device fabrication and allows straightforward deposition of the active layer using conventional solution-based processes.

3.3.2. Energy Transfer

The energy transfer from the host to the dye and subsequent emission from the dye can be due to several different processes such as Förster and Dexter energy transfer reactions as depicted in **Figure 3.7**.

Förster energy transfer is an efficient non-radiative energy transfer process which involves a dipole-dipole coupling of the transition dipole moments for the excited host or donor and the dye or acceptor in its ground state.[15] When an excited donor/exciton relaxes, its energy is transferred via a strong Coulombic interaction with a dye molecule. The dye molecule then emits this energy as light with the appropriate color and high luminance. The rate of the energy transfer relative to the radiative relaxation of the donor molecule determines whether the light emitted from the whole layer is exclusively from the dye dopant or from both host and dopant molecules.

$$k_{ET} \propto R_{DA}^{6}$$

where k_{ET} is the rate of energy transfer and R_{DA} is the distance between two dipole, μ_D and μ_A. It is clear that the efficiency of Förster transfer is highly dependent on the average molecular

spacing.

An alternative process for energy transfer is the Dexter energy transfer which involves an electron exchange mechanism with singlet-to-singlet and triplet-to-triplet transitions.[16] In this process, simultaneous or consecutive electron transfers lead the donor to its ground state and the acceptor to its electronic excited state. It essentially involves diffusion of excitons from donor to acceptor.

For Förster/Dexter energy transfer the separation of the host-guest molecules is of prime importance and it will correspond to an optimal dye concentration of ~1% for fluorescent dyes and ~10% for phosphorescent dyes.[17] The fluorescent dyes can only utilize singlet states via Förster energy transfer, while phosphorescent dyes can utilize singlet as well as triplet states via Dexter energy transfer. Utilization of singlets as well as triplets leads to a tremendous increase in the efficiency of the device.

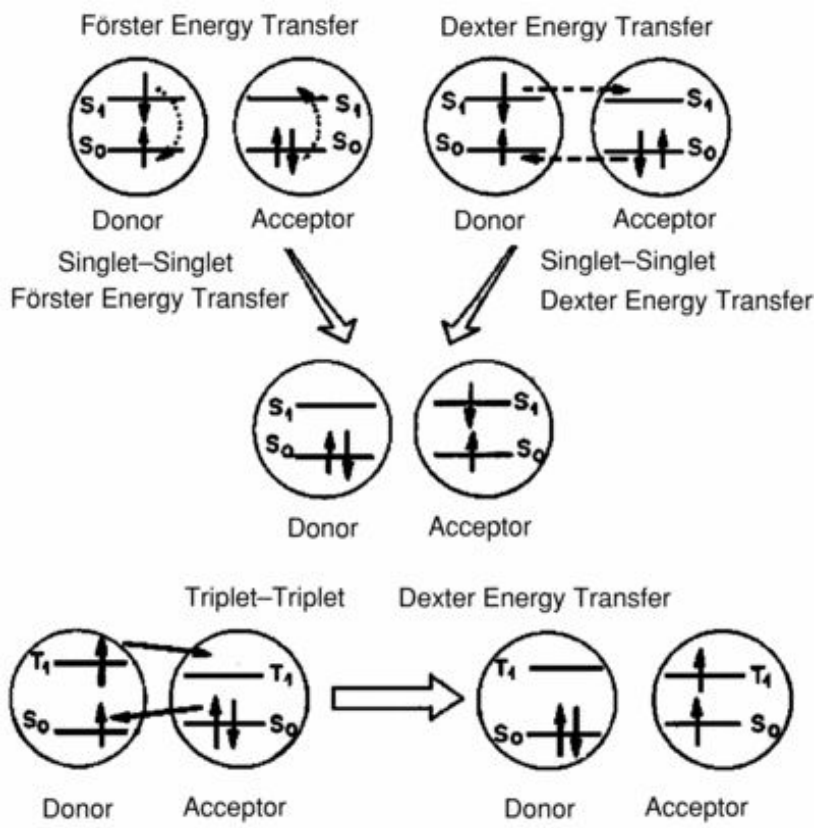

Figure 3.7. Förster/Dexter energy transfer.

3.4. References

[1] Destriau, G. 1936, 'Recherches sur les scintillations des sulfures de zinc aux rayons', *Journal de Chemie Physique*, vol. 33, p. 587-625.

[2] Tang, C. W. & Vanslyke, S. A. 1987, 'Organic electroluminescent diodes', *Applied Physics Letters*, vol. 51, no. 12, pp. 913-5.

[3] Heeger, A. J., Parker, I. D. & Yang, Y. 1994, 'Carrier injection into semiconducting polymers: Fowler-Nordheim field-emission tunneling', *Synthetic Metals*, vol. 67, no. 1-3, pp. 23-9.

[4] Parker, I. D. 1994, 'Carrier tunneling and device characteristics in polymer light-emitting diodes', *Journal of Applied Physics*, vol. 75, no. 3, pp. 1656-66.

[5] Tang, C. W., Vanslyke, S. A. & Chen, C. H. 1989, 'Electroluminescence of doped organic thin films', *Journal of Applied Physics*, vol. 65, no. 9, pp. 3610-6.

[6] Zhang, X. & Jenekhe, S. A. 2000, 'Electroluminescence of multicomponent conjugated polymers. 1. Roles of polymer/polymer interfaces in emission enhancement and voltage-tunable multicolor emission in semiconducting polymer/ polymer heterojunctions', *Macromolecules*, vol. 33, no. 6, pp. 2069-82.

[7] Kalinowski, Jan 2005, *Organic light-emitting diodes : Principles, characteristics, and processes* Marcel Dekker, New York.

[8] Campbell, I. H. & Smith, D. L. 1999, 'Schottky energy barriers and charge injection in metal/Alq/metal structures', *Applied Physics Letters*, vol. 74, no. 4, pp. 561-3.

[9] Ha, Y. Kim and C.-S. 2008, *Advances in Organic Light-Emitting Device*, Trans Tech Publications Ltd.

[10] Dodabalapur, Ananth 1997, 'Organic light emitting diodes', *Solid State Communications*, vol. 102, no. 2-3, pp. 259-67.

[11] *Commission Internationale de L'eclairage (CIE), method of measureing and specifying colour redering properties of light sources*, 1974.

[12] *Commission Internationale de L'eclairage (CIE), Colorimetry*, 1986.

[13] Kido, J., Hongawa, K., Okuyama, K. & Nagai, K. 1994, 'White light-emitting organic electroluminescent devices using the poly(N-vinylcarbazole) emitter layer doped with three fluorescent dyes', *Applied Physics Letters*, vol. 64, no. 7, pp. 815-7.

[14] D'Andrade, B. W. & Forrest, S. R. 2004, 'White organic light-emitting devices for solid-state lighting', *Advanced Materials*, vol. 16, no. 18, pp. 1585-95.

[15] Forster, Th 1959, '10th Spiers Memorial Lecture. Transfer mechanisms of electronic excitation', *Discussions of the Faraday Society*, vol. 27, pp. 7-17.

[16] Dexter, D. L. 1953, 'A theory of sensitized luminescence in solids', *The Journal of Chemical Physics*, vol. 21, no. 5, pp. 836-50.

[17] Misra, A., Kumar, P., Kamalasanan, M. N. & Chandra, S. 2006, 'White organic LEDs and their recent advancements', *Semiconductor Science and Technology*, vol. 21, no. 7, pp. R35-R47.

CHAPTER 4
HIGH PERFORMANCE ORGANIC OPTOELECTRONIC DEVICES ENHANCED BY SURFACE PLASMON RESONANCE

4.1 Introduction

Organic optoelectronic devices are regarded as promising technology that may be environmentally friendly renewable energy resources and the next generation flat-panel display platform.[1-3] Significant efforts over the last decade have been made to improve the efficiency of polymer-based optoelectronic devices using a variety of different processing strategies, such as better understanding of the device physics,[4-7] new materials for high performance,[8-11] optimization of the morphologies by advanced processing methods,[12-16] and advanced device architectures.[17-19] However, the performance of these devices is not yet up to the level for commercialization, and further enhancement is required for practical applications.

One approach to improve the efficiency of OSCs is to promote photon absorption inside the organic thin film. To increase absorption in the organic layer, a thicker active layer is inevitable, resulting in increased device resistance which is attributed to low carrier mobility. From this perspective, the surface plasmon resonance (SPR) can be an effective approach to enhance the photogeneration of excitons, resulting in light trapping by increasing the photon absorption efficiency of the organic materials with the incorporation of plasmonic nanomaterials in the photovoltaic devices, while keeping their optical thickness. For organic light-emitting diodes (OLEDs), generally, the incorporation of metal nanoparticles into the devices is known to induce emission quenching via a Förster-type energy transfer between the emitter and the metal nanoparticles.[20-22]

Surface plasmons are waves associated with strongly enhanced electromagnetic fields occurring on the surface owing to their interaction with the free electrons of certain metals.[23] Metallic nanoparticles can be used as sub-wavelength antennas, in which the plasmonic near-field is coupled to the dielectric layer that stores the incident energy in a localized surface plasmon mode.[24] Enhanced fields are utilized for plasmon-enhanced absorption in the active layer of OSCs and result in a higher photocurrent.[25-28] For OLEDs, an improvement in the overall performance is obtained due to the enhanced photoluminescence (PL) and acceleration of the radiative process from SPR wavelengths near metal nanoparticles. [21,29-31]

The purpose of experiment of this chapter is to demonstrate the surface plasmon effect on OSCs and OLEDs containing interfacial metal nanoparticles such as copper, gold, and copper-gold alloy

between indium tin oxide (ITO) and poly(3,4-ethylenedioxylenethiophene):polystyrene sulfonic acid (PEDOT:PSS). A polystyrene-*block*-poly(2-vinylpyridine) (PS-*b*-P2VP) copolymer template was used to make arrays of metal nanoparticles. We found that bimetallic nanostructures as well as pure metal nanoparticles induce the SPR effect in the optoelectronic devices. Increased light absorption of the polymer thin layer with the incorporation of metallic nanostructures was demonstrated, resulting in higher efficiency compared to conventional optoelectronic devices. Notably, the spectrum range of the enhanced light absorption corresponds to the individual SPR region of the metal nanoparticles. The significant SPR effect in the optoelectronic devices, which shows enhancement of more than 20%, is discussed in detail.

4.1.1 Surface Plasmon Resonance

Surface plasmon resonance (SPR) on metal nanoparticles is a strong enhancement of the local electromagnetic field compared to the exciting electromagnetic field. A metal nanoparticle can be as a resonator for surface plasmons, if excited resonantly the oscillation amplitude can overcome the excitation amplitude by orders of magnitude.

An external electromagnetic field can penetrate into the volume of the metal nanoparticle and shift the free conduction electrons with respect to the particles' metal ion lattice. The resulting surface charges of opposite sign on the opposite surface elements of the particles produce a restoring local field within the particle.

Two primary schemes are commonly explained for SPR. Surface plasmon polaritons (SPPs) propagating along the metal dielectric interface are triggered by incorporating metallic nanostructures. The other one is localized surface plasmon resonance (LSPR) by metallic nanoparticles such as Cu, Ag, Au.[32] The LSPR is achieved when the frequency of the incident light matches its resonance peak, resulting in unique optical properties which are selective light extinction as well as local enhancement of electromagnetic field near the metallic particles surface. (**Figure 4.1**) The resonance peak depends on the size, shape, and the dielectric environment of the metal nanoparticles.

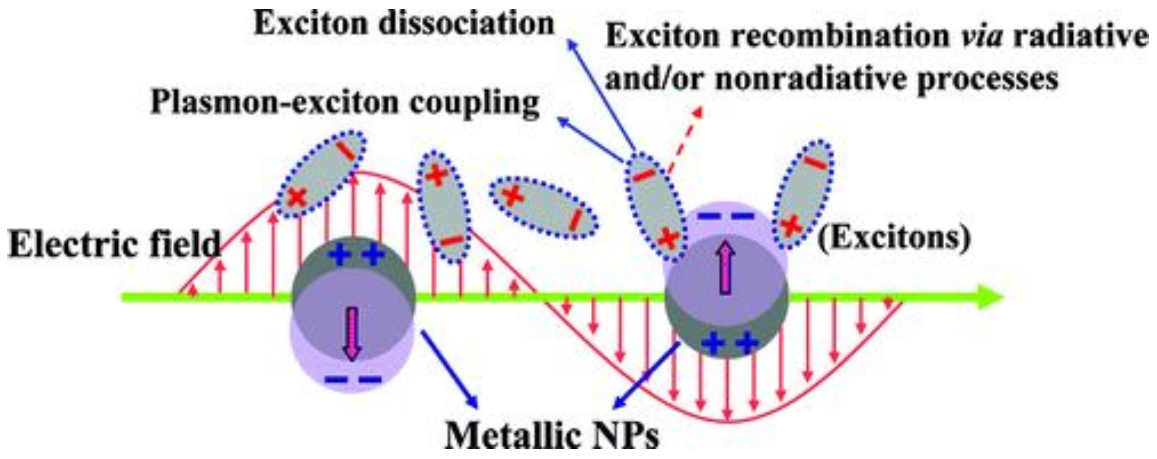

Figure 4.1. Simple schematic of localized surface plasmon resonance.

4.2 Experiment

4.2.1 Devices Preparation

The poly(3-hexyltihophene):[6,6]-phenyl-C61 butyric acid methyl ester (P3HT:PCBM) bulk heterojunction system was studied for OSCs with the configuration indium thin oxide (ITO)/metal nanoparticles/poly(3,4-ethylenedioxylenethiophene):polystyrene sulfonic acid (PEDOT:PSS)/P3HT:PCBM/Al. Poly(2-methoxy-5-(2-ethyl-hexyloxy)-1,4-phenylene vinylene) (MEH-PPV) was used for emission material of OLEDs inserting barium between MEH-PPV and Al electrode with same configuration of OSCs. Before the fabrication of the devices, the ITO-coated glass substrate was cleaned by ultrasonic treatment using detergent, deionized water, acetone, and isopropyl alcohol in sequence and dried in an oven for 24 h. The metal nanoparticles are embedded on the ITO substrate using by polystyrene-*block*-poly(2-vinylpyridine) (PS-*b*-P2VP) block copolymer. On top of metal nanoparticles layer, the PEDOT:PSS was spin cast at 5000rpm for 40s, and then dried at 140˚C for 10min in air. For OSCs, an active layer composed of 2wt% P3HT:PCBM blend (1:1) in 1,2-dichlorobenzene was spin cast at 700rpm in a N_2-filled glovebox and the electrodes (Al) was deposited on the active layer in vacuum ($<10^{-7}$ Torr) thermal evaporator. For OLEDs, an emission layer of 0.6wt% MEH-PPV in p-xylene was spin coated at 1500rpm and the electrodes (Ba/Al) was evaporated on the emissive layer at same condition with OSCs.

4.2.2 Synthesis of Metal nanoparticles

To synthesize the metal nanoparticles, polystyrene-*block*-poly(2-vinylpyridine) (PS-*b*-P2VP) block copolymer (M_n^{PS} = 133 kg/mol, M_n^{P2VP} = 132 kg/mol, M_w/M_n = 1.05) was purchased from Polymer Source and used it without further purification. The copolymer was dissolved in toluene to make 0.4 wt% polymer solution, a selective solvent for PS blocks, to create spherical micelles composed of a P2VP core and a PS corona at room temperature, and then hydrogen tetrachloroaurate ($HAuCl_4$) and copper chloride ($CuCl_2$) was added to the solution with molar ratio of 0.8 (metal to pyridyl unit), keeping stirring over 12 hrs at room temperature. Subsequently, the metal-containing polymer solution was spin-coated at 4000 rpm for 40 sec onto the cleaned ITO substrate and followed by H_2 plasma etching at 50 W for 20 min.

4.2.3 Device Characteristics

For characteristics of device, UV-vis absorption spectrum, PL measurement, atomic force microscopy, J-V characteristics and EQE were measured.

UV-Vis absorption spectra were measured on a Varian Cary 5000 spectrophotometer and PL measurements were carried out using a He-Cd laser operating at a wavelength of 325nm. Surface patterns of block copolymer and nanoparticles were imaged using atomic force microscopy (Nanoscope V, Veeco) in tapping mode. The Current density-voltage (*J-V*) characteristics of OSCs were measured using a Keithley 2635A Source Measure Unit. Solar cell performance utilized an Air Mass 1.5 G (AM 1.5 G) solar simulator with an irradiation intensity of 100 mW cm^{-2}. External quantum efficiency (EQE) measurements were obtained by using the PV measurements OE system applied monochromatic light from a xenon lamp under ambient conditions. The monochromatic light intensity was calibrated with a Si photodiode and chopped at 100Hz. Masks (13.5mm^2) made of thin metal were attached to each cell before measurement for *J-V* characteristics and EQE. The electrical properties of the OLEDs were measured using a Keithley 2400 source measurement unit equipped with Minolta CS2000 under ambient conditions.

4.3 Results and Discussion

4.3.1 Atomic Force Microscopy

The height mode force microscopic (AFM) images are shown in **Figure 4.2.** In **Figure 4.2a, b** PS-*b*-P2VP micellar thin films containing with Au precursors that molar ratio of Au to the pyridyl unit is 0.8 and Au nanoparticles prepared by a plasma treatment after removing block copolymer templates. The as-spun film of block copolymer incorporated with metal nanoparticle precursors shows a short range order and an average separation distance of 100 nm. When these films were

exposed to hydrogen (H_2) plasma for 20 min, metal salts were converted to pure metal nanoparticles with an average diameter of 20 nm without changing the separation distance, while all polymers were completely degraded under the same condition. In addition, Cu nanoparticles and Au-Cu alloy arrays with similar dimensions were prepared in the same manner, as shown in **Figure 4.2c** and **Figure 4.2d**.

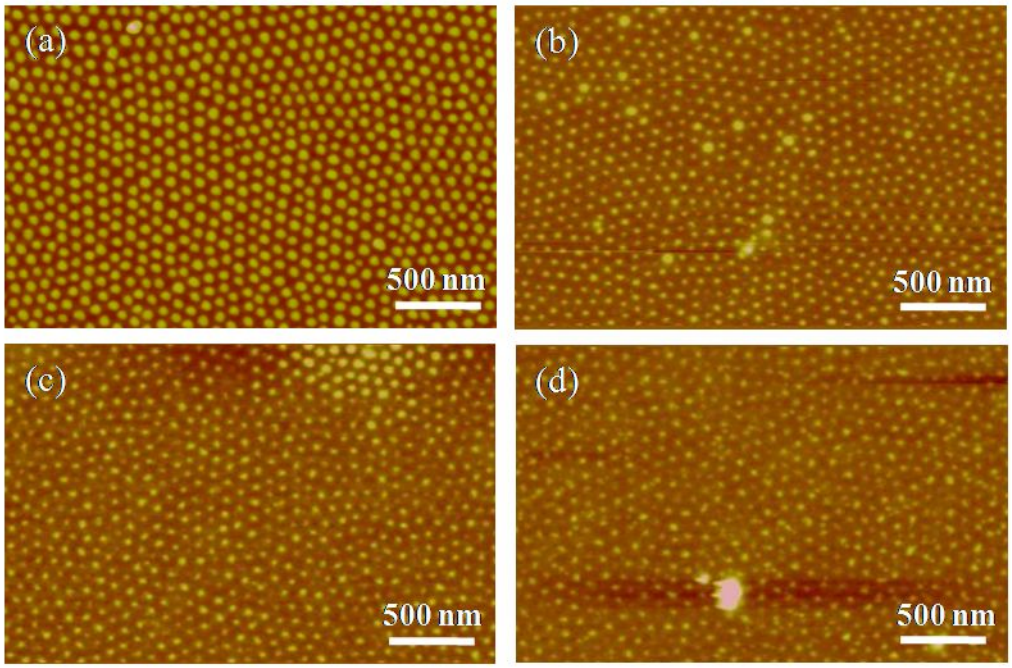

Figure 4.2. Height mode AFM images of (a) gold-containing PS-*b*-P2VP copolymer thin films (b) gold (Au) nanoparticle (c) copper (Cu) nanoparticle and (d) Au-Cu alloy arrays.

4.3.2 UV-Vis Spectroscopy and Simulated Spectrum

To confirm of the SPR characteristics of the nanoparticles, the UV-Vis absorption spectra of the nanoparticles were investigated in a thin film deposited onto ITO glass, as depicted in **Figure 4.3**. These three metal nanoparticles, pure copper (Cu), gold (Au), and Cu-Au alloy, show a broad absorption peak around 600 nm, 540 nm, and 580 nm, respectively, arising from the SPR of each nanoparticle. In the case of Cu-Au alloy, the absorption peak is shifted along with broad absorbance maxima in the range of 550-600nm, the intermediate position between Au and Cu. This indicates that the nanoparticles are a bimetallic form of Au and Cu.[33] Given that same amount of Au and Cu precursors were loaded onto the P2VP core in the copolymer templates and were subsequently reduced by H_2 plasma, both the Cu and Au nanoparticles are uniformly mixed within the same nanoparticles with an average diameter of 20 nm.

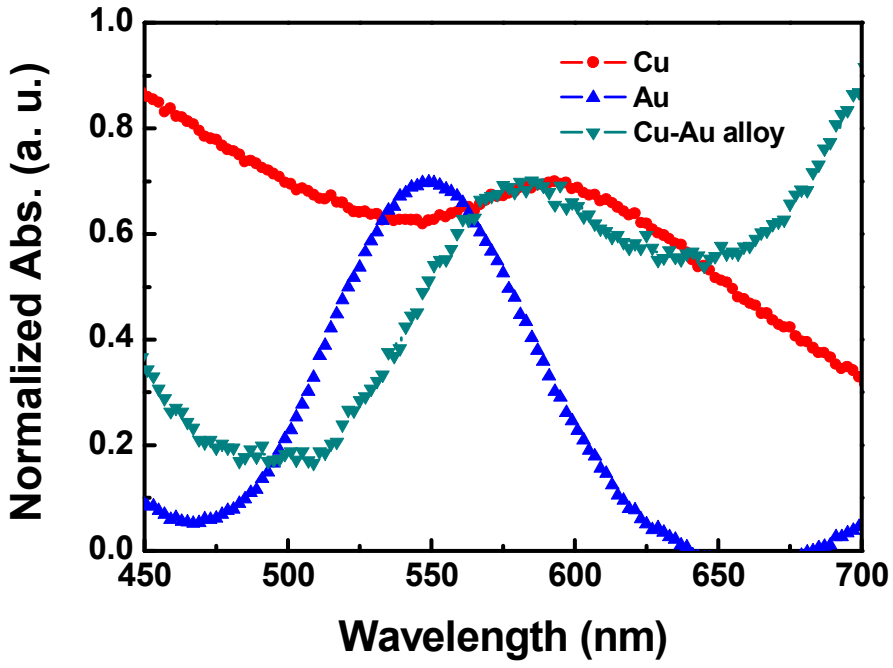

Figure 4.3. Normalized UV-Vis absorption spectra of pure Cu, Au and Cu-Au alloy metal nanoparticles.

To elucidate the UV-Vis absorption spectra of the nano particles, a three dimensional finite-difference time-domain (FDTD) method was used to theoretically model the optical response of the nanoparticle array. **Figure 4.4** shows simulated extinction spectra of the hexagnoal Au ,Cu, and Au-Cu nanoparticle array with the diameter of 25 nm and the height of 20 nm. The calculated spectra widths are smaller than the experimental ones, which indicates the size ditribution in the nanoparticles. However, it clearly shows that the experiment and calculation agree well in terms of the shape and location of the localized surface plasmon resonance (LSPR) at about 567 nm, 582 nm and 572 nm for the Au, Cu, and Au-Cu nanoparticle array, respectively. Also, the near-field intensity distribution shown in the inset of **Figure 4.4** reveals the electromagnetic field enhancement around the Au nanoparticle due to the LSPR.

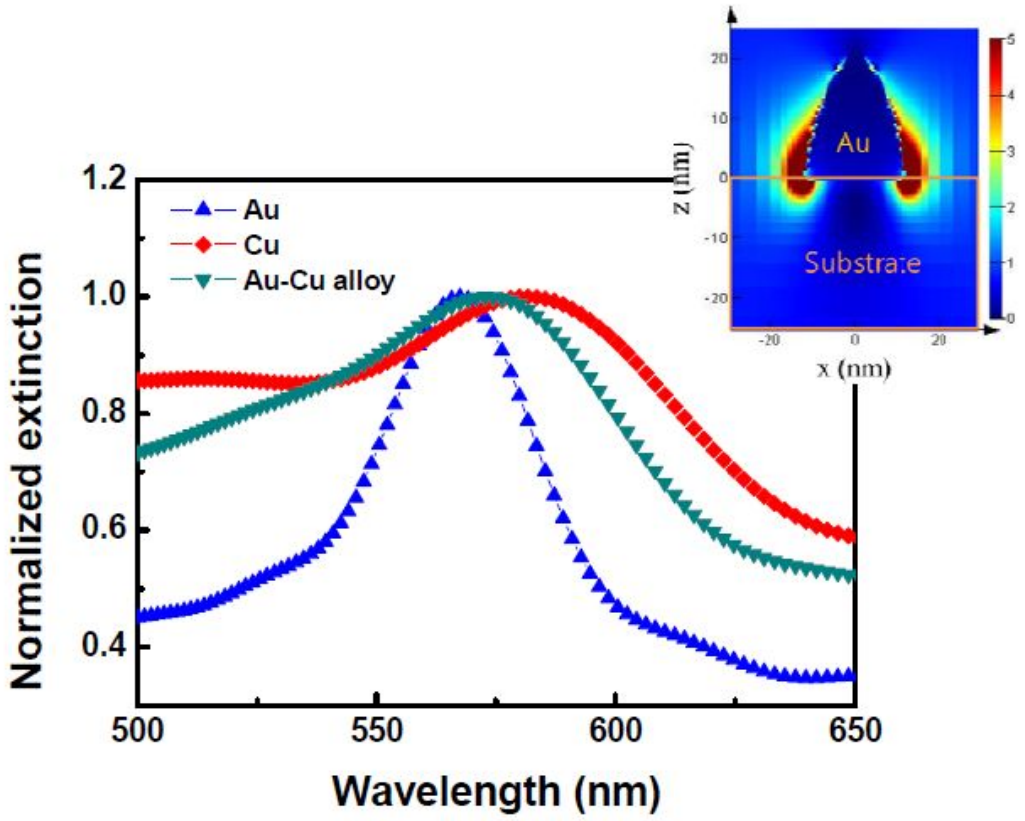

Figure 4.4. Simulated normalized extinction spectrum for the Au, Cu and Cu-Au nanoparticle array. The inset shows normalized field distirbution $|E|$ of Au nanoparticle for illumination at resonance (λ=567 nm).

4.3.3 Photoluminescence

To investigate the SPR effect on the PL emission of metallic structure, the PL spectra of MEH-PPV layer with and without each metal nanoparticles were measured, as shown in **Figure 4.5**. Polymer layer embedded with metal nanoparticles shows relatively stronger PL intensity compared to the film without a metallic particle. This PL intensity enhancement is due to the SPR effect on the emission layer through the metal nanoparticles, which can lead to increased absorption of the incident light by concentrating the a local electromagnetic hot spot. The fluorescence process is dependent on the light excitation rate and the quantum yield, which is dependent on competition between the radiative and nonradiative decaying mechanisms.[34] Because the resonance frequency of the metal nanoparticles was close to the absorption band of MEH-PPV, we attribute the enhanced PL intensity to the fact that excitation of the SPR increased the degree of light absorption and, thereby, enhanced the light excitation rate.

Enhanced PL was observed with a well-matched spectral overlap between the SPR wavelength of the nanoparticles and the excitation peak of the MEH-PPV. This fact can be evident that these metal nanoparticles are suitable for OLEDs using MEH-PPV, as their optical absorption peak is located in a broad region from 500 to 650nm, which suitably overlaps the emissive layer at 580nm.

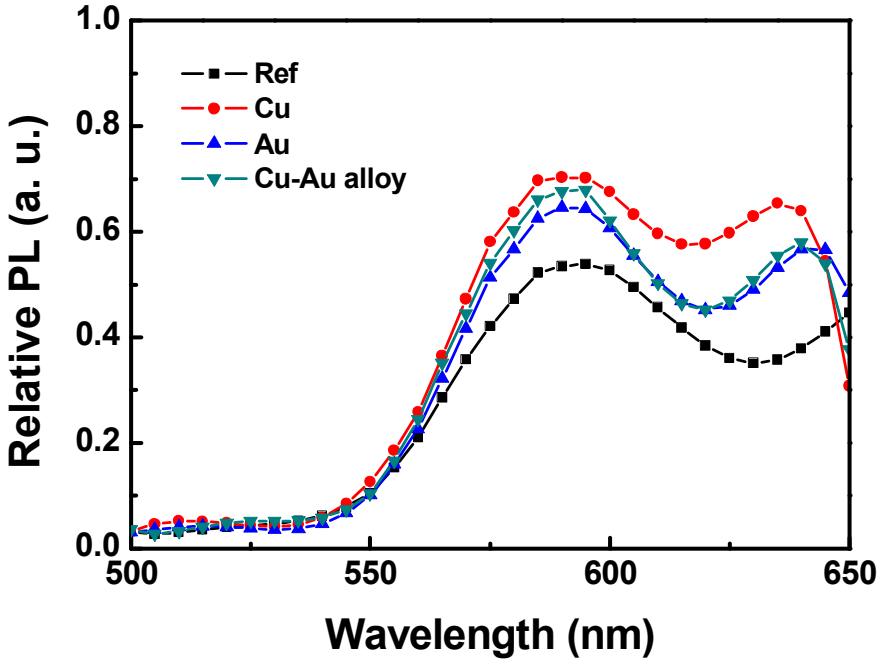

Figure 4.5. Normalized PL spectra of MEH-PPV layer with and without metal nanoparticles.

4.3.4 J-V Characteristics for OSCs and OLEDs

4.3.4.1 OSCs Characteristics

Under simulated AM 1.5 G illumination, the *J-V* characteristics of the devices are shown in **Figure 4.6**, with their performance summarized in **Table 1**.The devices modified with metal nanoparticles had a positive effect on the PSC performance, including a significant improvement of J_{SC}, while other parameters such as the V_{OC} and the *FF* were similar to those of the reference device. Similar V_{OC} and *FF* both with and without metal nanoparticles are not crucial factors in the cell performance due to the SPR effect. The J_{SC} with the pure Cu, Au, and Cu-Au alloy device were 9.60, 8.50, and 9.37 mA cm^{-2} with ~20%, 5%, and 16% enhancement, respectively, compared to the reference device (8.08 mA cm^{-2}). This indicates that the improvement in the J_{SC} can be attributed to the SPR effect of the metal nanoparticles. To ascertain the specific reason for this increased J_{SC}, the EQE was determined in each device. It is clear that the substantial enhancement of the J_{SC} with metal particles as reflected by the higher EQE values follow the same *J-V* characteristics. The calculated J_{SC} values from EQE of the devices with Cu, Au, and Cu-Au alloy were 9.23, 8.69, and 9.29, respectively, as compared to the reference value (8.18 mA cm^{-2}). Each device with Cu and Au nanoparticles formed on top of the ITO was observed a ~13% and ~6% EQE enhancement around a spectral range from 450 nm to 650 nm with Cu and from 400 nm to 600 nm with Au, respectively. Furthermore, a bimetallic device can cover a wavelength of 400 nm to 650 nm with a ~14% increase in the total EQE, including a plasmon resonance peak at 580 nm. As the EQE depends on the amount of absorption, it is clear that the observed enhancement of the J_{SC} leading to enhanced optical absorption can be attributed to the surface plasmon excitation of the metal nanoparticles.

	J_{SC} (mA cm^{-2})	V_{OC} (V)	FF (%)	η (%)	Calculated J_{SC} (mA cm^{-2})
Reference	8.08	0.60	0.60	2.90	8.18
Cu MNPs	9.60	0.58	0.58	3.22	9.23
Au MNPs	8.50	0.58	0.60	2.98	8.69
Cu-Au MNPs	9.37	0.58	0.61	3.35	9.29

Table 1. Summary of typical OSCs parameters with and without metallic layer.

(a)

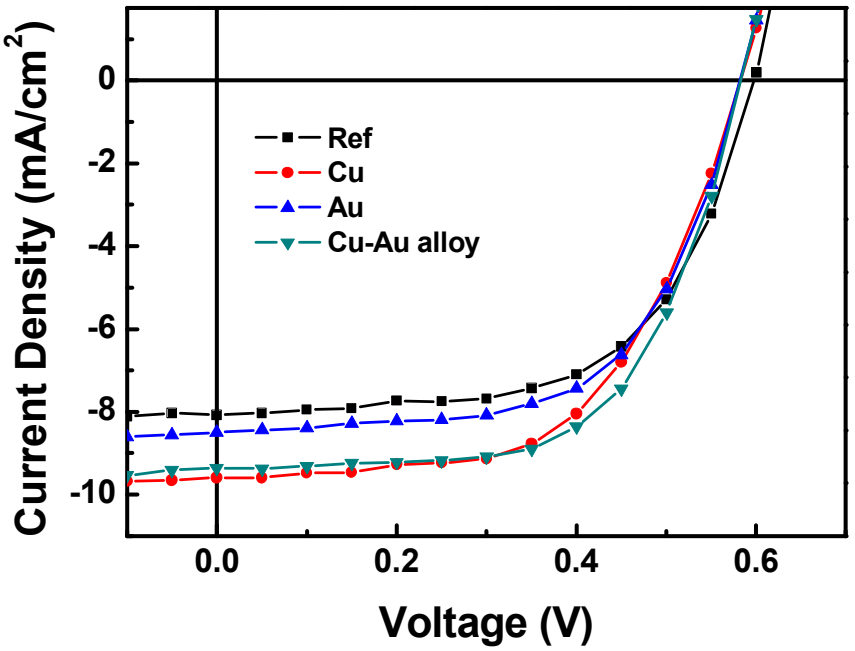

(b)

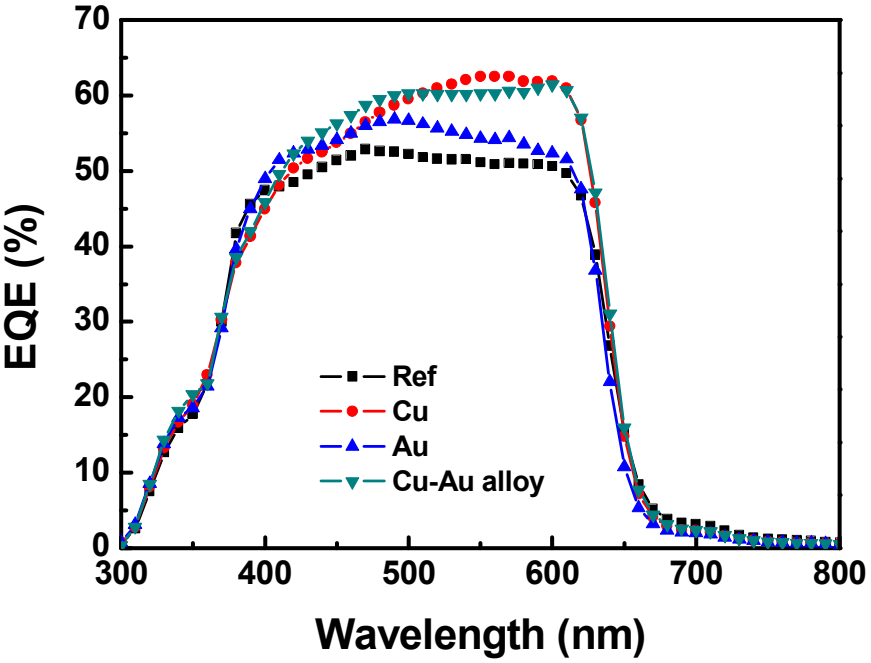

Figure 4.6. OSCs characteristics of (a) *J-V* characteristics and (b) EQE spectra of metal nanoparticle devices.

4.3.4.2 OLEDs Characteristics

The device performances of metal-embedded PLEDs are presented in **Figure 4.7**, and the detailed characteristics are summarized in **Table 2**. The devices modified with metal nanoparticles show higher performance compared to the reference device without metal nanoparticles (16932 mA cm^{-2} at 5.6V). The maximum luminance of the pure Cu, pure Au, and the Cu-Au alloy device were 22636 (at 6.4V), 22268 (at 6.2V), and 20973 mA cm^{-2} (at 6.4V), respectively, and the luminous efficiency corresponds to approximately 12~24% of the enhanced results, while the turn-on voltages of all devices were identical at 2.2V. Therefore, the improved performance observed in the devices prepared with metal nanoparticles can be explained in terms of surface plasmon-assisted radiative recombination acceleration caused by the metal nanoparticles. This enhancement is attributed to the maintenance of proper separation between the metal structure supporting the plasmons and the light-emitting molecule by the dielectric material layer, which suppresses the energy transfer process resulting in destroying the excited states. As a result, spectral overlapping of the emitter band and the SPR band of the metal nanoparticles led to an increase in the radiative decay rate and affected the performance of the device.

Device configuration	Maximum luminance (cd/m^2) (at voltage)	Maximum luminous efficiency (cd/A) (at voltage)	Turn on voltage (V)
ITO/PEDOT:PSS/MEH-PPV/Ba/Al	16932 (5.6V)	1.40 (4.2V)	2.2
ITO/Cu/PEDOT:PSS/MEH-PPV/Ba/Al	22636 (6.4V)	1.74 (5.8V)	2.2
ITO/Au/PEDOT:PSS/MEH-PPV/Ba/Al	22268 (6.2V)	1.61 (5.4V)	2.2
ITO/Alloy/PEDOT:PSS/MEH-PPV/Ba/Al	20973 (6.4V)	1.57 (5.4V)	2.2

Table 2. Summary of typical OLEDs parameters with and without metallic layer.

(a)

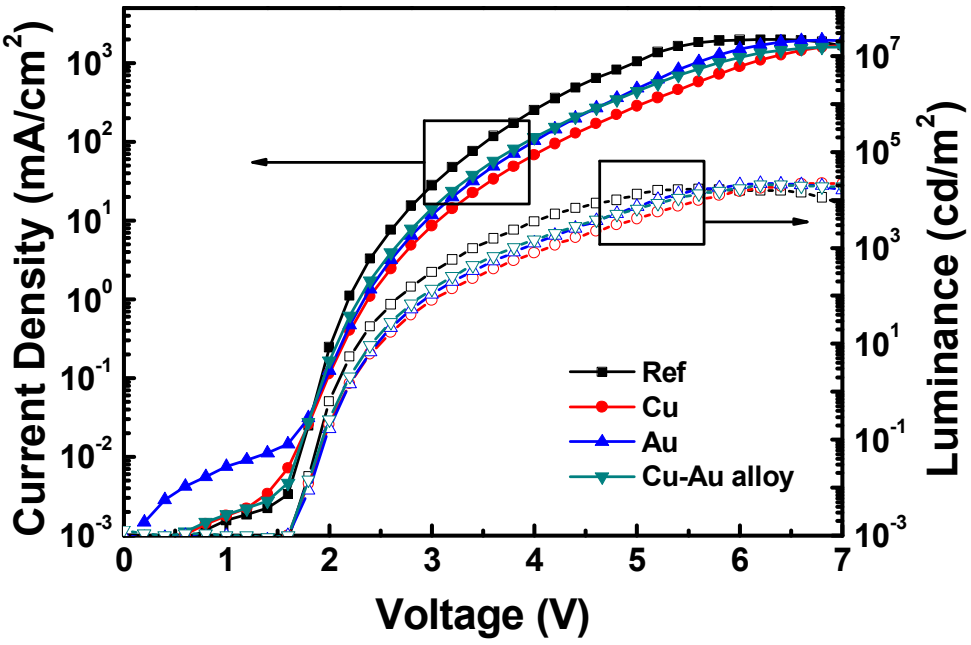

(b)

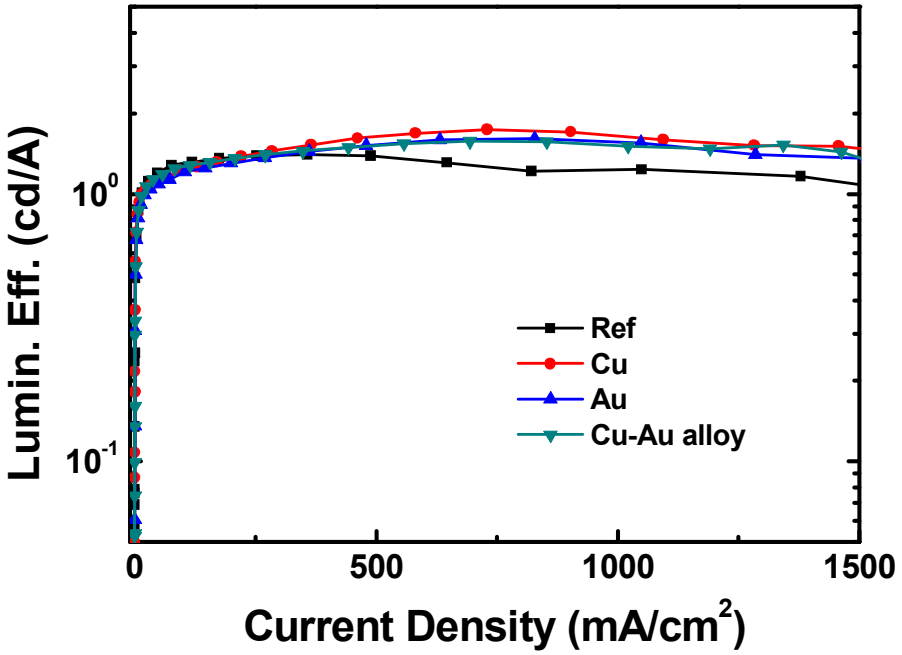

Figure 4.7. OLEDs characteristics of (a) current density vs. applied voltage *(J-V)*, luminance vs. applied voltage *(L-V)* and (b) luminous efficiency vs. current density *(LE-J)* curves with and without metal nanoparticles.

4.4 Conclusions

In this chapter, enhanced performance of metal-embedded optoelectronic devices was demonstrated due to the SPR effect of metal nanoparticles. To incorporate the metallic structure on the device, a simple solution processable casting method is used by a block copolymer template.

Attributed to the SPR effect, for the OSCs, , enhancement of the J_{SC} value for Cu, Au, and Cu-Au alloy devices was approximately ~20%, 5%, and 16%, respectively, compared to a reference device. With the same trend, the EQE was also observed increased value at each SPR wavelength of the metal nanoparticles.

For OLEDs, an enhanced luminescence and efficiency through the embedded metal nanoparticles were observed attributed to suppresse the energy transfer process by SPR. Due to this effect, increased efficiency was obtained in optoelectronic devices. The results of the experiment on these plasmonic nanocomposite systems confirm that SPR is promising for use in the development of high-performance organic optoelectronic devices.

4.5. References

[1] Yu, G., Gao, J., Hummelen, J. C., Wudl, F. & Heeger, A. J. 1995, 'Polymer photovoltaic cells: Enhanced efficiencies via a network of internal donor-acceptor heterojunctions', *Science*, vol. 270, no. 5243, pp. 1789-91.

[2] Brabec, C. J., Sariciftci, N. S. & Hummelen, J. C. 2001, 'Plastic solar cells', *Advanced Funtional Materials*, vol. 11, no. 1, pp. 15-26.

[3] Burroughes, J. H., Bradley, D. D. C., Brown, A. R., Marks, R. N., Mackay, K., Friend, R. H., Burns, P. L. & Holmes, A. B. 1990, 'Light-emitting diodes based on conjugated polymers', *Nature*, vol. 347, no. 6293, pp. 539-41.

[4] Parker, I. D. 1994, 'Carrier tunneling and device characteristics in polymer light-emitting diodes', *Journal of Applied Physics*, vol. 75, no. 3, pp. 1656-66.

[5] Blom, P. W. M., Mihailetchi, V. D., Koster, L. J. A. & Markov, D. E. 2007, 'Device physics of polymer:Fullerene bulk heterojunction solar cells', *Advanced Materials*, vol. 19, no. 12, pp. 1551-66.

[6] Park, S. H., Roy, A., Beaupré, S., Cho, S., Coates, N., Moon, J. S., Moses, D., Leclerc, M., Lee, K. & Heeger, A. J. 2009, 'Bulk heterojunction solar cells with internal quantum efficiency approaching 100%', *Nature Photonics*, vol. 3, no. 5, pp. 297-303.

[7] Deibe, C., Strobe, T. & Dyakonov, V. 2010, 'Role of the charge transfer state in organic donor-acceptor solar cells', *Advanced Materials*, vol. 22, no. 37, pp. 4097-111.

[8] Chen, H. Y., Hou, J., Zhang, S., Liang, Y., Yang, G., Yang, Y., Yu, L., Wu, Y. & Li, G. 2009, 'Polymer solar cells with enhanced open-circuit voltage and efficiency', *Nature Photonics*, vol. 3, no. 11, pp. 649-53.

[9] Liang, Y., Xu, Z., Xia, J., Tsai, S. T., Wu, Y., Li, G., Ray, C. & Yu, L. 2010, 'For the bright future-bulk heterojunction polymer solar cells with power conversion efficiency of 7.4%', *Advanced Materials*, vol. 22, no. 20, pp. E135-E8.

[10] Zhao, Guangjin, He, Youjun & Li, Yongfang 2010, '6.5% Efficiency of Polymer Solar Cells Based on poly(3-hexylthiophene) and Indene-C60 Bisadduct by Device Optimization', *Advanced Materials*, vol. 22, no. 39, pp. 4355-8.

[11] Chen, L., Zhang, B., Cheng, Y., Xie, Z., Wang, L., Jing, X. & Wang, F. 2010, 'Pure and saturated red electroluminescent polyfluorenes with dopant/host system and PLED efficiency/color purity trade-offs', *Advanced Functional Materials*, vol. 20, no. 18, pp. 3143-53.

[12] Lee, T. W. & Park, O. O. 2000, 'Effect of different heat treatments on the luminescence efficiency of polymer light-emitting diodes', *Advanced Materials*, vol. 12, no. 11, pp. 801-4.

[13] Shi, Y., Liu, J. & Yang, Y. 2000, 'Device performance and polymer morphology in polymer light emitting diodes: The control of thin film morphology and device quantum efficiency', *Journal of Applied Physics*, vol. 87, no. 9 I, pp. 4254-63.

[14] Jo, J., Kim, S. S., Na, S. I., Yu, B. K. & Kim, D. Y. 2009, 'Time-dependent morphology ewolution by annealing processes on polymer:Fullerene blend solar cells', *Advanced Functional Materials*, vol. 19, no. 6, pp. 866-74.

[15] Moulé, A. J. & Meerholz, K. 2009, 'Morphology control in solution-processed bulk-heterojunction solar cell mixtures', *Advanced Functional Materials*, vol. 19, no. 19, pp. 3028-36.

[16] Hoven, C. V., Dang, X. D., Coffin, R. C., Peet, J., Nguyen, T. Q. & Bazan, G. C. 2010, 'Improved performance of Polymer bulk heterojunction solar cells through The reduction of phase separation via solvent additives', *Advanced Materials*, vol. 22, no. 8, pp. E63-E6.

[17] Kim, J. Y., Kim, S. H., Lee, H. H., Lee, K., Ma, W., Gong, X. & Heeger, A. J. 2006, 'New architecture for high-efficiency polymer photovoltaic cells using solution-based titanium oxide as an optical spacer', *Advanced Materials*, vol. 18, no. 5, pp. 572-6.

[18] Kim, J. Y., Lee, K., Coates, N. E., Moses, D., Nguyen, T. Q., Dante, M. & Heeger, A. J. 2007, 'Efficient tandem polymer solar cells fabricated by all-solution processing', *Science*, vol. 317, no. 5835, pp. 222-5.

[19] Song, M. H., Kabra, D., Wenger, B., Friend, R. H. & Snaith, H. J. 2009, 'Optically-pumped lasing in hybrid organic-inorganic light-emitting diodes', *Advanced Functional Materials*, vol. 19, no. 13, pp. 2130-6.

[20] Park, J. H., Lim, Y. T., Park, O. O., Kim, J. K., Yu, J. W. & Kim, Y. C. 2004, 'Polymer/Gold Nanoparticle Nanocomposite Light-Emitting Diodes: Enhancement of Electroluminescence Stability and Quantum Efficiency of Blue-Light-Emitting Polymers', *Chemistry of Materials*, vol. 16, no. 4, pp. 688-92.

[21] Choulis, S. A., Mathai, M. K. & Choong, V. E. 2006, 'Influence of metallic nanoparticles on the performance of organic electrophosphorescence devices', *Applied Physics Letters*, vol. 88, no. 21, pp. 213503/1-3.

[22] Wu, J. L., Chen, F. C., Hsiao, Y. S., Chien, F. C., Chen, P., Kuo, C. H., Huang, M. H. & Hsu, C. S. 2011, 'Surface plasmonic effects of metallic nanoparticles on the performance of polymer bulk heterojunction solar cells', *ACS Nano*, vol. 5, no. 2, pp. 959-67.

[23] Barnes, W. L., Dereux, A. & Ebbesen, T. W. 2003, 'Surface plasmon subwavelength optics', *Nature*, vol. 424, no. 6950, pp. 824-30.

[24] Atwater, H. A. & Polman, A. 2010, 'Plasmonics for improved photovoltaic devices', *Nature Materials*, vol. 9, no. 3, pp. 205-13.

[25] Kim, K. & Carroll, D. L. 2005, 'Roles of Au and Ag nanoparticles in efficiency enhancement of poly(3-octylthiophene)/C60 bulk heterojunction photovoltaic devices', *Applied Physics Letters*, vol. 87, no. 20, pp. 203113/1-3.

[26] Morfa, A. J., Rowlen, K. L., Reilly Ii, T. H., Romero, M. J. & Van De Lagemaat, J. 2008, 'Plasmon-enhanced solar energy conversion in organic bulk heterojunction photovoltaics', *Applied Physics Letters*, vol. 92, no. 1, pp. 013504/1-3.

[27] Lee, J. H., Park, J. H., Kim, J. S., Lee, D. Y. & Cho, K. 2009, 'High efficiency polymer solar cells with wet deposited plasmonic gold nanodots', *Organic Electronics: physics, materials, applications*, vol. 10, no. 3, pp. 416-20.

[28] Yoon, W. J., Jung, K. Y., Liu, J., Duraisamy, T., Revur, R., Teixeira, F. L., Sengupta, S. & Berger, P. R. 2010, 'Plasmon-enhanced optical absorption and photocurrent in organic bulk heterojunction photovoltaic devices using self-assembled layer of silver nanoparticles', *Solar Energy Materials and Solar Cells*, vol. 94, no. 2, pp. 128-32.

[29] Chen, Y., Munechika, K. & Ginger, D. S. 2007, 'Dependence of fluorescence intensity on the spectral overlap between fluorophores and plasmon resonant single silver nanoparticles', *Nano Letters*, vol. 7, no. 3, pp. 690-6.

[30] Chowdhury, S., Bhethanabotla, V. R. & Sen, R. 2009, 'Silver-copper alloy nanoparticles for metal enhanced luminescence', *Applied Physics Letters*, vol. 95, no. 131115/1-3.

[31] Yang, B., Lu, N., Qi, D., Ma, R., Wu, Q., Hao, J., Liu, X., Mu, Y., Reboud, V., Kehagias, N., Torres, C. M. S., Boey, F. Y. C., Chen, X. & Chi, L. 2010, 'Tuning the intensity of metal-enhanced fluorescence by engineering silver nanoparticle arrays', *Small*, vol. 6, no. 9, pp. 1038-43.

[32] Kelly, K. L., Coronado, E., Zhao, L. L. & Schatz, G. C. 2003, 'The optical properties of metal nanoparticles: The influence of size, shape, and dielectric environment', *Journal of Physical Chemistry B*, vol. 107, no. 3, pp. 668-77.

[33] Itakura, T., Torigoe, K. & Esumi, K. 1995, 'Preparation and characterization of ultrafine metal particles in ethanol by UV irradiation using a photoinitiator', *Langmuir*, vol. 11, no. 10, pp. 4129-34.

[34] Anger, P., Bharadwaj, P. & Novotny, L. 2006, 'Enhancement and quenching of single-molecule fluorescence', *Physical Review Letters*, vol. 96, no. 11, pp. 113002/1-4.

CHAPTER 5
A FIRST APPROACH TO WHITE ORGANIC ELECTROLUMINESCENCE DEVICE FROM A SINGLE ROD-COIL POLY[THIOPHENE-BLOCK-(N-VINYLCARBAZOLE)] DIBLOCK COPOLYMER

5.1 Introduction

OLEDs that emit white light are of interest and potential importance for use in active matrix display and for solid state lighting.[1] In such applications, the fabrication of large-area devices and the use of low-cost manufacturing technology will be the major issues.[2] Several approaches have been used to generate white light from OLEDs.[3-5]

Simply, it can be divided into two schemes to generate WOLEDs. One scheme to emit white light from small phosphorescent molecules in multilayer structured devices.[6-8] In this configuration, the lumiphores in each layer of the device can either be excited directly by electron hole recombination in their respective layer or they can be excited by an energy transfer process from neighboring layers. In order to obtain balanced excitation by direct recombination, thin hole and electron blocking layer are usually inserted in between the emissive layers.[9] However, one of the drawbacks of this scheme is that the emission spectrum usually changes according to the applied bias to the device is increased because the resulting increase in the internal electric field has a different effect on the kinetics of electrons and holes.

Another approach to white emission is to use doped or blended polymeric systems with different fluorescent or phosphorescent materials.[10-12] Doping the matrix material with one or several lumiphores risks that the blend phase-separates over time which will result in film inhomogeneities, shifts in the color of the emitted light, and a local increase in current density.[13,14] Due to their generally lower miscibility, polymeric materials are particular prone to this effect. One way to overcome any phase separation is to develop a single-component covalently link all components of the white-emitting blend. For example, this can be achieved by copolymerizing the components into a single white-emitting copolymer.

Block copolymers allow self-assembling control over the spatial location of their functional component blocks as well as various objects,[15-19] resulting in the unique potential to allure for organic electronic applications. Recently, It was not only reported the synthesis of a rod-coil block copolymer containing electron and hole transporting blocks but also showed the improved OLED

performance due to the controlled solid-state morphology.[20] Moreover, Fre´chet and coworkers have also demonstrated the use of diblock copolymers as active materials for WOLEDs in which the incorporation of heavy Ir(III) metal complexes within the polymer backbone must be accompanied to generate a white emission.[21]

In this chapter, the synthesis of a rod-coil diblock copolymer incorporating a low bandgap polymeric block (regioregular poly(3-hexylthiophene) (P3HT) and a wide bandgap chromophore [poly(N-vinylcarbazole) (PVK) tethered to a coil-like backbone (P3HT-b-PVK)] through living polymerization strategy is demonstrated. We report here an unprecedented example of nearly ‘‘pure’’ white emission with CIE coordination of (0.34, 0.33) fabricated from the single metal free-based diblock copolymer.

5.2 Experiment

5.2.1 Synthesis of P3HT-*b*-PVK

Trithiocarbonate terminated P3HT as a macro-RAFT agent (0.10 g, ~12mmol estimated by GPC) and AIBN (0.75 mg, 4.5μmol) as an initiator, and anhydrous toluene (2.5 mL) were mixed in a Schlenk flask which was purged with argon for 15 min. To this solution, a mixture of N-vinylcarbazole (1.2 g, 6.21 mmol) and anhydrous toluene (3 mL) was added and degassed by freeze–pump–thaw cycles (3x), flushed with dry argon. The mixture was immersed in oil bath at 70 8C for 24 h. The polymer solution was transferred centrifuge tube, precipitated with MeOH (200 mL), centrifuged, and decanted. The crude product was treated with MeOH twice in the same manner. The resulting solid was filtered off and subjected to sequential Soxhlet extraction with MeOH (1 d) and acetone (1 d) to remove the trace amount of uncreative P3HT and *N*-vinylcarbazole monomer. After redissolving in THF, the polymer was again precipitated into MeOH, centrifuged, decanted, washed with MeOH, and dried in vacuo to give a reddish solid polymer. ^{1}H NMR ($CDCl_3$, 600 MHz) : δ (ppm) = 7.97–7.77 (br, m), 7.21–6.77 (br, m), 6.67–6.1 (br, m), 5.1–4.7 (br, m), 2.87–2.65 (br, m), 1.81–1.63 (br, m), 1.55–1.17 (br, m), 0.97–0.81(br, m). GPC analysis M_n = 13800 g mol^{-1}, M_w = 21400 kg mol^{-1}, and PDI = 1.55 (against PS standard).

5.2.2 Device Fabrication

The single-layer block copolymer light emitting diode with the configuration indium tin oxide (ITO)/poly(3,4-ethylenedioxylenethiophene):polystyene sulfonic acid (PEDOT:PSS)/poly[thiophene-block-(N-vinylcarbazole)] diblock copolymer (P3HT-b-PVK)/Ba/Al was fabricated. Before the fabrication of the devices, the ITO-coated glass substrate was cleaned by ultrasonic treatment using detergent, deionized water, acetone, and isopropyl

alcohol in an ultrasonic bath. The substrates were subsequently dried in an oven at ~100ºC for 12h before treatment with UV-ozone. The PEDOT:PSS was spin-cast at 4000rpm for 40s, after treatment with UV-ozone for 15min, and followed by drying on a hotplate at 140ºC for 10min in air. On top of PEDOT:PSS layer, P3HT-*b*-PVK block copolymer of 1wt% in chlorobenzene was spin coated at 700rpm in a N_2-filled glovebox. Top electrodes (Ba/Al) were deposited on the emissive block copolymer single layer in a vacuum ($<10^{-7}$ Torr) thermal evaporator.

5.2.3 Device Characteristics

All solvents were purified and freshly distilled prior to use. The trithiocarbonate terminated P3HT (macro-RAFT agent) was prepared in literature procedures.[22] ^{1}H NMR spectra were recorded on a Varian FT-NMR 600MHz spectrometer and referenced to the solvent peak. UV–Vis absorption spectra were measured in chlorobenzene solution on a Varian Cary 5000 spectrophotometer. The current density (*J*), voltage (*V*), luminance (*L*), electroluminescence (EL) spectrum and Commission Internationale de 1'Eclairage (CIE) coordinates were measured using a Keithley 2365A source measurement unit equipped with Minolta CS2000 under ambient conditions. Emission and excitation photoluminescence (PL) spectra were obtained by Edinburgh spectrometer in solution in quartz cuvette under ambient condition.

5.3 Results and Discussion

5.3.1 Analysis of ^{1}H NMR

A narrow polydispersity trithiocarbonate macro-RAFT agent based on P3HT (H/trithiocarbonate) (Mn = 8.3 kg mol^{-1}, PDI = 1.11, against PS standard) was prepared via the slightly synthetic modification of the method previously developed by McCullough and coworkers.[23] Rod-coil poly(thiophene-*block*-(*N*-vinylcarbazole)) diblock copolymer (P3HT-b-PVK) with *N*-vinylcarbazole was synthesized via RAFT polymerization. (**Figure 5.1**) A major shift in the GPC trace was observed toward higher molecular weight with a monomodal molecular weight distribution, indicating well controlled block copolymer formation.

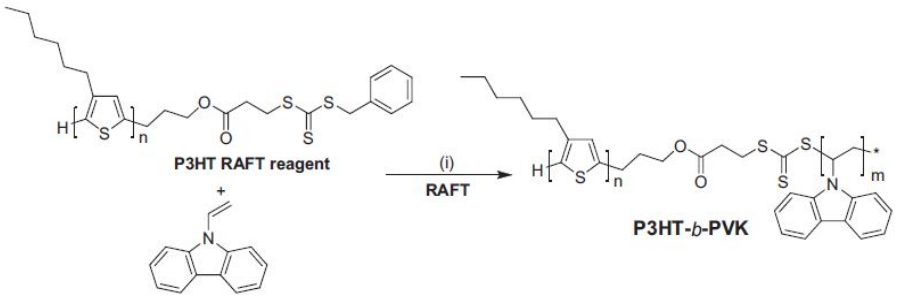

Figure 5.1. Synthesis of P3HT-*b*-PVK (Reagent and conditions: AIBN, toluene, 70 8C, 24 h).

After purification, the GPC analysis of P3HT-*b*- PVK exhibits Mn = 13.8 kg mol^{-1} with PDI = 1.55 (THF, PS standard). An inspection of the ^{1}H NMR spectrum of P3HT-*b*-PVK shows typically characteristic chemical shifts from P3HT blocks (H-*a* for the thiophene C*H*, H-*b* for the methylene of the *n*-hexyl group nearest the thiophene and H-*c* toH-*g* related to residual alkyl chains) as well as PVK blocks (seen as broad complex configuration signals from 8.2 to 4.3 ppm). (**Figure 5.2**) Note that the asymmetrical PVK resonances (*o*-*h*) are displayed in the ^{1}H NMR despite the fact the carbazole moiety belongs to the C_{2v} symmetry group.[24,25] This nonequivalence in PVK has been previously reported, which is attributed to restricted rotation of the bulky carbazole combined with ring current effects of neighboring rings. The structural composition (P3HT/ PVK = 44.6:55.4 mol-%) for P3HT-*b*-PVK is estimated by integrating the aromatic carbazole protons (H-*k* and H-*l*) against the methylene protons of the thiophene (H-*a*) in the ^{1}H NMR.

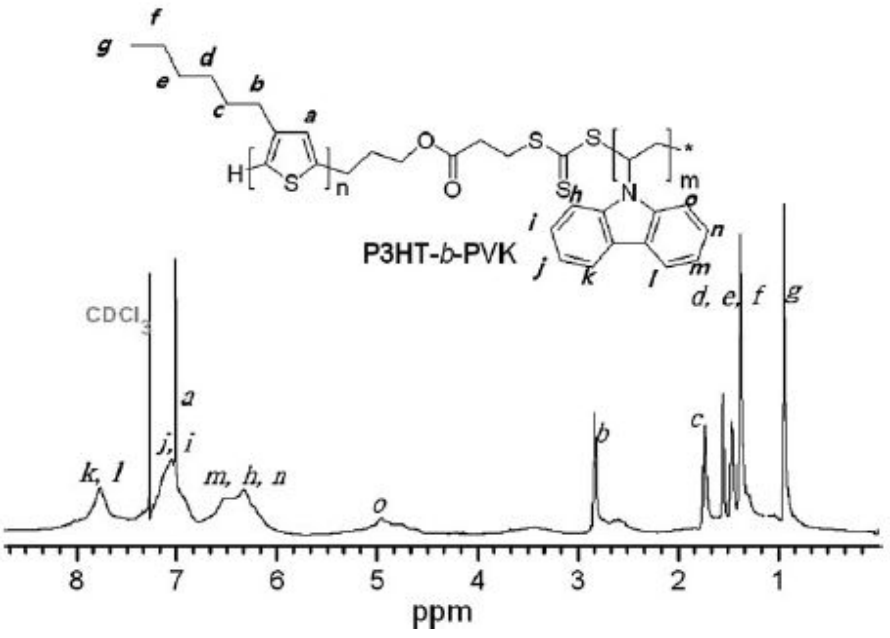

Figure 5.2. ^{1}H NMR spectrum of P3HT-*b*-PVK recorded at room temperature in $CDCl_3$.

5.3.2 UV-Vis spectroscopy

To understand properties of this new polymer, the UV-Vis spectroscopy was investigated in chlorobenzene solution and in thin films. The film was prepared on quartz uniformly by spin coaing method from their respective chlorobenzene solutions at room temperature. There are two dominant absorption bands with 344 and 452nm. For the lower energy peak at 452nm, this feature is arising due to π-π^* transition from P3HT block, while the band at 344nm with a vibronic phenomenon is clearly assigned to the PVK segment. The observation of optical characteristics of the individual building blocks in electronic absorption of P3HT-*b*-PVK is an indication of the absence of any ground state interaction between the thiophene and the carbazole chromophores, leading to the display of their individual absorption features. The optical absorption of a physical blend of P3HT and PVK at 45:55w/w% of which composition is similar to that of the block copolymer is shown in **Figure 5.3**, indicating that the absorption spectrum of the diblock is superposition of those of the homopolymers. Upon examining P3HT-*b*-PVK in the solid state, the copolymer film shows a less resolved broad peak centered at 537nmwhich is characteristic of the P3HT blocks, while the vibrationally resolved high-energy band in the 330–347 region attributed to the PVK segments reveals almost indistinguishable absorption spectra in the solution and in the films.

It is interesting to point out, that for the characteristic band of P3HT in the copolymer P3HT-b-PVK is only broadening and bathochromically shifted when moving from the solution to solid state. This suggests the notion that a form of packing crystallographic rearrangement of the PVK blocks in the copolymer can be excluded in the solid state. One can be expected that such a different conformation between rigid rod-like P3HT and flexible coil-like PVK blocks in the copolymer film is capable of a nanophase separation behavior.

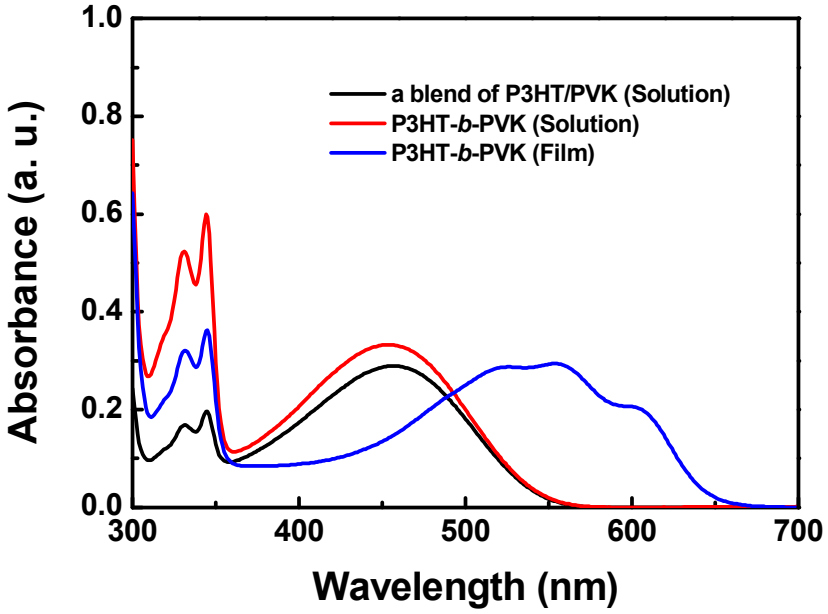

Figure 5.3. UV–Vis absorption spectra of P3HT-*b*-PVK and a physical mixture of identical P3HT/PVK (45:55 w/w%) in chlorobenzene solution and in thin film.

5.3.3 Photoluminescence

The PL spectra of P3HT-*b*-PVK both in solution and thin film not only show a large blue emission peak of 410nm maximum wavelength due to PVK units but also a broad reddish emission band centered at 580nm without the well resolved vibrational energy bands reveals, when excited at 330nm. (**Figure 5.4**) The PL feature of P3HT-*b*-PVK in the film is nearly identical to that in solution, but a similar interesting observation can be seen regarding the broadening of the P3HT bands resulting from P3HT chromophore solid-state packing, which is good consistent with UV–Vis data described above. It has been confirmed that there is different morphology within each individual component on the copolymer when going from solution to the solid state. Besides, the absence of any significant quenching of emission from the higher energy PVK blocks indicates that there is no efficient intrachain and interchain energy migration from PVK to P3HT, as a result of the emitting isolation of two chromophores, resulting in individual emissions from each segment. The Förster energy transfer typically occurs at distances below 10nm between two chromophores. Thereby, the individual emissions from P3HT-*b*-PVK that consists of P3HT and PVK blocks connected via saturated spacer of 2nm, currently lacks a logical explanation. It is probably attributed either to the site isolation of chromophores within appropriately sized polymer domains,[21,26] non-radiative energy transfer in the blocks,[27,28] or both.

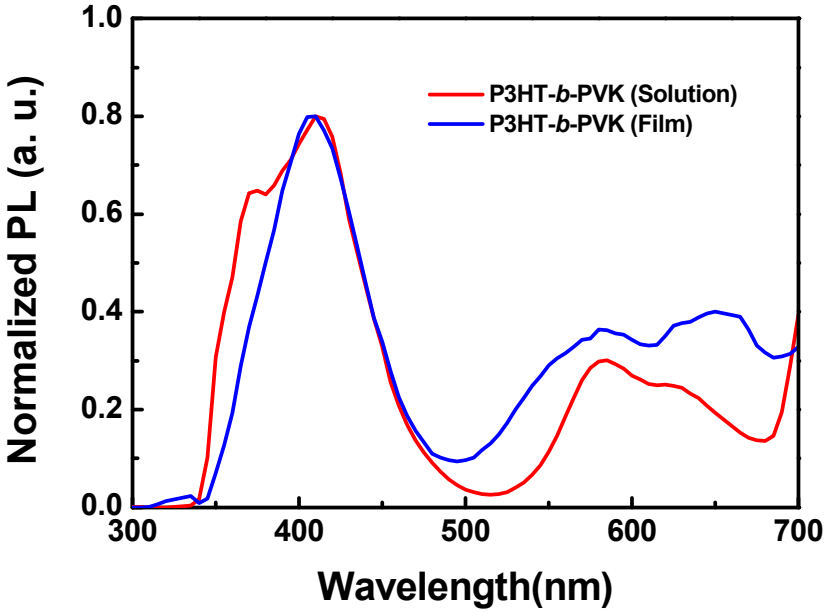

Figure 5.4. Photoluminescence spectra of P3HT-*b*-PVK (λ_{exc} = 330 nm) in chlorobenzene solution and in thin film.

5.3.4 Atomic Force Microscopy

Figure 5.5 shows the topography and phase images of the P3HT-*b*-PVK film cast from chlorobenzene. For AFM analysis, the unexpected optical behavior of P3HT-*b*-PVK can be understood the by their unusual surface morphology. Typical features are clearly visualized by AFM as well defined micron-sized nano fiberlike structures with up to a length of 120nm and an average diameter of ca. 7nm, confirming the microphase-separated diblocks. Note that the slow evaporation after spin-casting procedure was necessary to allow the P3HT-*b*-PVKto form a fibrillar morphology.

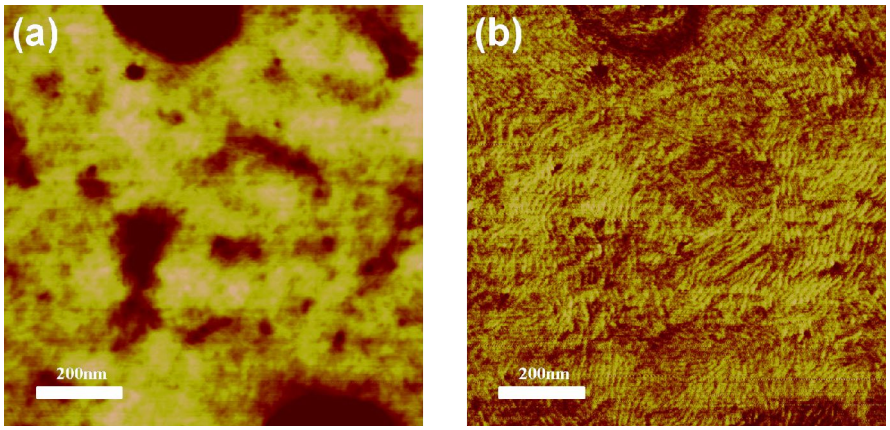

Figure 5.5. (a) Atomic force microscopy (AFM) topographic image and (b) the corresponding phase image of P3HT-b-PVK film.

5.3.5 Electroluminescence

It is of considerable interest to explore the differences in the properties of electroluminescent device characteristics between the block copolymer and the P3HT/PVK physical blend at 45:55 w/w% since it enables us to access the influence of the limited energy transfer in the block copolymer in comparison with the blending system on OLEDs. The PVK/P3HT blended OLED displays one dominant emission band at 650nm with a shoulder at 710nm originated from P3HT segments. The nearly complete quenching of emission from the higher energy PVK blocks points out that the lower energy P3HT block acts as a quantum well which traps excitons and acts as

radiative recombination units. In contrast to the blended homopolymeric system, the EL spectrum of P3HT-b-PVK consists of two distinct peaks at 410 and 575 nm, which is similar to that of the PL in the film. The presence of the 410nm band due to PVK block emission is clearly suggestive that the energy transfer is almost ruled out in the P3HT-*b*-PVK. A rationale for this phenomenon is that the phase separated domains through controlling the nanoscale of the block copolymer is critical to suppress energy transfer from high to low energy by isolating the trithiocarbonate units as inert spacer between the blocks. This notion is indeed good consistent with Eland AFM data described above. Notably, in contrast, for the rod-coil block copolymer, energy migration is much less efficient, also resulting in blue-shifted emission relative to the pure conjugated P3HT.[29] (**Figure 5.6**) It can be assumed, despite the fact that the creation of the micro separated diblocks is observed in the AFM phase image, and the relatively constrained P3HT segments in the block copolymer reduce the ordered structure of P3HT packing when compared to that of P3HT in blended system.

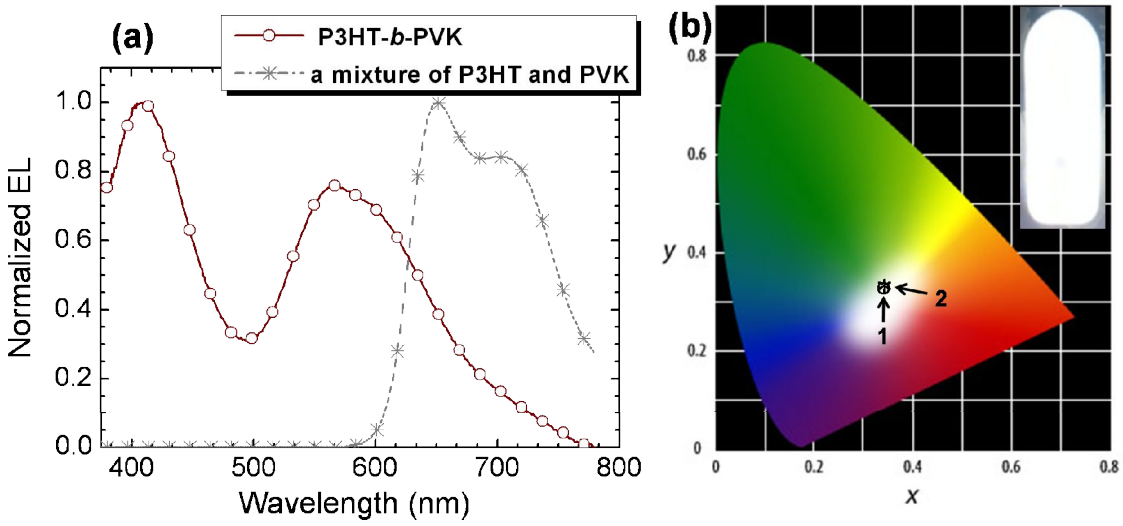

Figure 5.6. (a) Electroluminescence (EL) spectra for the block copolymer (–o–) and a mixture with P3HT/PVK ratio of 45:55 w/w% (–*–), respectively. (b) CIE chromaticity diagram showing the ordinates of standard white light (point 1) and white-light emitting film of P3HT-b-PVK (point 2). Inset is a photograph of device operated under 10 V.

5.3.6 Characteristics of WOLEDs

By virtue of this minimized energy transfer, the P3HT-*b*-PVK is capable of producing a white emission through a combination of two different chromophores emitting blue and orange/red. Under a driving voltage of 10 V, a pure white emission is achieved with maximum luminance of 130 cd m^{-2} as shown in **Figure 5.8**. The emission color of the device fabricated from P3HT-*b*-PVK is located very close to equi-energy point in the CIE chromaticity diagram and shows only a slight dependence on voltage change: the CIE coordinates varied from (0.34, 0.33) to (0.35, 0.34) over a voltage range of 8–10 V. (**Figure 5.7**)

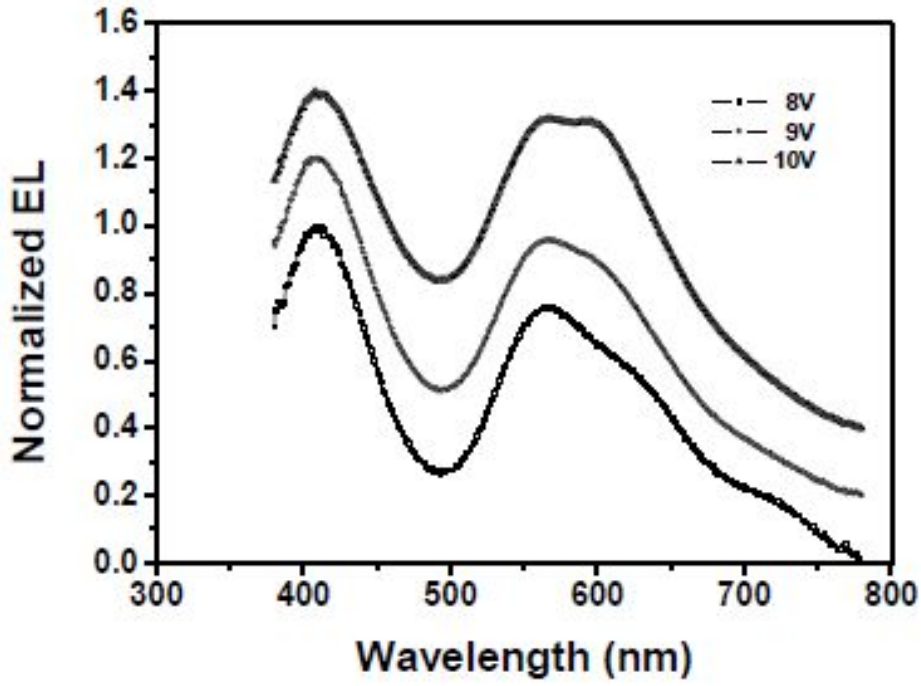

Figure 5.7. EL spectra of P3HT-*b*-PVK film under various voltages.

(a)

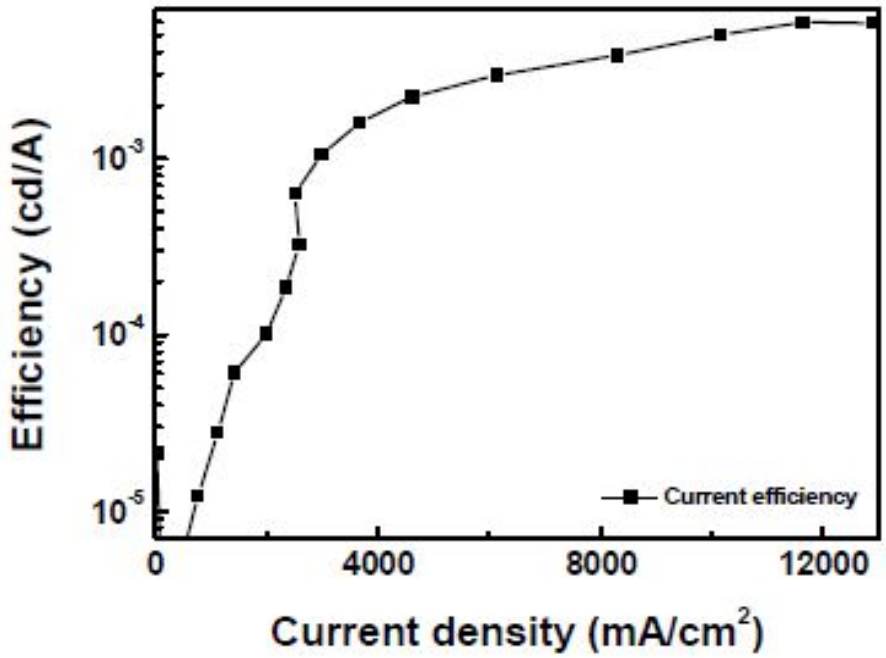

(b)

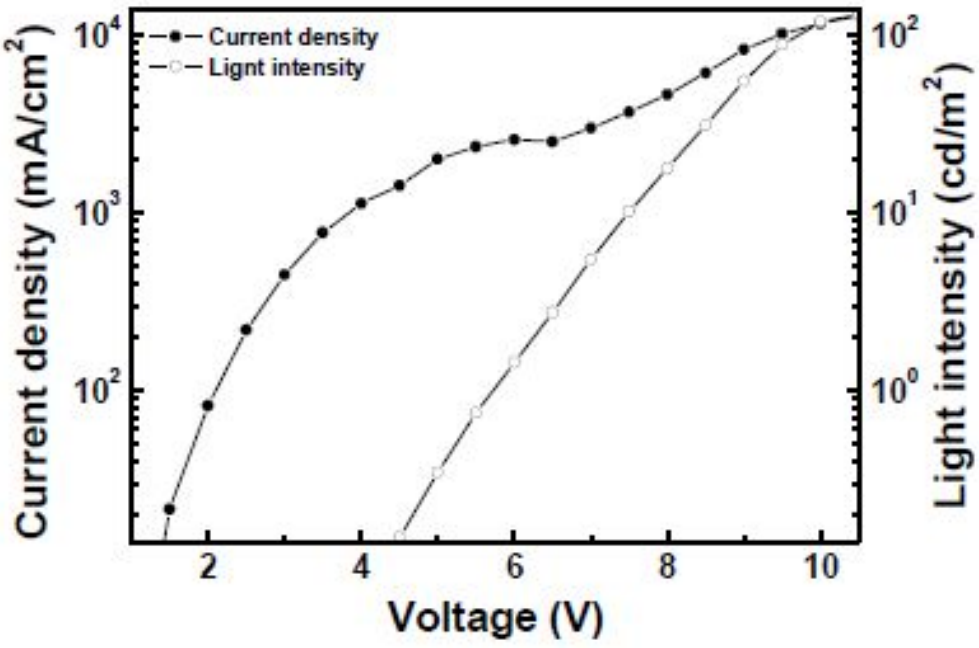

Figure 5.8. (a) Current density and luminance plotted against applied electric field *(J-V-L)*, and (b) Current efficiency plotted against current density for the device P3HT-*b*-PVK.

5.4 Conclusions

In this chapter, a rod-coil block copolymer comprising P3HT as low bandgap segments and PVK as wide bandgap blocks (P3HT-*b*-PVK) has been synthesized by synthetic strategy of RAFT polymerization. The film morphology of the P3HT-*b*-PVK explored by AFM study elucidates a phase separated nanofibrilar structure, leading to dual emissions produced by each individual chromophore P3HT and PVK. As a result of combination of blue and orange/red emission from the isolated bichromophoric blocks, the EL device of the resulting block copolymer is capable of generating direct white light with the CIE coordinates of (0.34, 0.33). While the performance of the block copolymer may appears to be relatively low, it must be emphasized that this is the first white emission with a single block copolymer that does not engaged with metal complexes, opening up new strategies for the development of WOLEDs.

5.5 References

[1] Heeger, A. J. 1998, 'Light emission from semiconducting polymers: Light-emitting diodes, light-emitting electrochemical cells, lasers and white light for the future', *Solid State Communications*, vol. 107, no. 11, pp. 673-9.

[2] D'Andrade, B. W. & Forrest, S. R. 2004, 'White organic light-emitting devices for solid-state lighting', *Advanced Materials*, vol. 16, no. 18, pp. 1585-95.

[3] Mu□ller, C. D., Falcou, A., Reckefuss, N., Rojahn, M., Wiederhirn, V., Rudati, P., Frohne, H., Nuyken, O., Becker, H. & Meerholz, K. 2003, 'Multi-colour organic light-emitting displays by solution processing', *Nature*, vol. 421, no. 6925, pp. 829-33.

[4] Shen, Z., Burrows, P. E., Bulović, V., Forrest, S. R. & Thompson, M. E. 1997, 'Three-color, tunable, organic light-emitting devices', *Science*, vol. 276, no. 5321, pp. 2009-11.

[5] Wang, Y. Z., Sun, R. G., Meghdadi, F., Leising, G. & Epstein, A. J. 1999, 'Multicolor multilayer light-emitting devices based on pyridine-containing conjugated polymers and para-sexiphenyl oligomer', *Applied Physics Letters*, vol. 74, no. 24, pp. 3613-5.

[6] Xu, X., Yu, G., Di, C., Liu, Y., Shao, K., Yang, L. & Lu, P. 2006, 'Efficient nondoped white organic light-emitting diodes based on electromers', *Applied Physics Letters*, vol. 89, no. 123503/1-3.

[7] Yan, B. P., Cheung, C. C. C., Kui, S. C. F., Xiang, H. F., Roy, V. A. L., Xu, S. J. & Che, C. M. 2007, 'Efficient white organic light-emitting devices based on phosphorescent platinum(II)/fluorescent dual-emitting layers', *Advanced Materials*, vol. 19, no. 21, pp. 3599-603.

[8] Park, Y. S., Kang, J. W., Kang, D. M., Park, J. W., Kim, Y. H., Kwon, S. K. & Kim, J. J. 2008, 'Efficient, color stable white organic light-emitting diode based on high energy level yellowish-green dopants', *Advanced Materials*, vol. 20, no. 10, pp. 1957-61.

[9] Kido, J., Kimura, M. & Nagai, K. 1995, 'Multilayer white light-emitting organic electroluminescent device', *Science*, vol. 267, no. 5202, pp. 1332-4.

[10] Ho, G. K., Meng, H. F., Lin, S. C., Homg, S. F., Hsu, C. S., Chen, L. C. & Chang, S. M. 2004, 'Efficient white light emission in conjugated polymer homojunctions', *Applied Physics Letters*, vol. 85, no. 20, pp. 4576-8.

[11] Xu, Y., Peng, J., Jiang, J., Xu, W., Yang, W. & Cao, Y. 2005, 'Efficient white-light-emitting diodes based on polymer codoped with two phosphorescent dyes', *Applied Physics Letters*, vol. 87, no. 19, pp. 193502/1-3.

[12] Gong, X., Wang, S., Moses, D., Bazan, G. C. & Heeger, A. J. 2005, 'Multilayer polymer light-emitting diodes: White-light emission with high efficiency', *Advanced Materials*, vol. 17, no. 17, pp. 2053-8.

[13] Tasch, S., List, E. J. W., Ekström, O., Graupner, W., Leising, G., Schlichting, P., Rohr, U., Geerts, Y., Schert, U. & Müllen, K. 1997, 'Efficient white light-emitting diodes realized with new processable blends of conjugated polymers', *Applied Physics Letters*, vol. 71, no. 20, pp. 2883-5.

[14] Lee, Y. Z., Chen, X., Chen, M. C., Chen, S. A., Hsu, J. H. & Fann, W. 2001, 'White-light electroluminescence from soluble oxadiazole-containing phenylene vinylene ether-linkage copolymer', *Applied Physics Letters*, vol. 79, no. 3, pp. 308-10.

[15] Bates, F. S. & Fredrickson, G. H. 1999, 'Block copolymers-designer soft materials', *Physics Today*, vol. 52, no. 2, pp. 32-8.

[16] Bockstaller, M. R., Mickiewicz, R. A. & Thomas, E. L. 2005, 'Block copolymer nanocomposites: Perspectives for tailored functional materials', *Advanced Materials*, vol. 17, no. 11, pp. 1331-49.

[17] Bang, J., Kim, S. H., Drockenmuller, E., Misner, M. J., Russell, T. P. & Hawker, C. J. 2006, 'Defect-free nanoporous thin films from ABC triblock copolymers', *Journal of the American Chemical Society*, vol. 128, no. 23, pp. 7622-9.

[18] Kim, B. J., Bang, J., Hawker, C. J. & Kramer, E. J. 2006, 'Effect of areal chain density on the location of polymer-modified gold nanoparticles in a block copolymer template', *Macromolecules*, vol. 39, no. 12, pp. 4108-14.

[19] Kim, B. J., Fredrickson, G. H., Hawker, C. J. & Kramer, E. J. 2007, 'Nanoparticle surfactants as a route to bicontinuous block copolymer morphologies', *Langmuir*, vol. 23, no. 14, pp. 7804-9.

[20] Tao, Y., Ma, B. & Segalman, R. A. 2008, 'Self-assembly of rod-coil block copolymers and their application in electroluminescent devices', *Macromolecules*, vol. 41, no. 19, pp. 7152-9.

[21] Poulsen, B. D. A., Kim, B. J., Biwu, M., Sebastian Zonte, C. & Fréchet, J. M. J. 2010, 'Site isolation in phosphorescent bichromophoric block copolymers designed for white electroluminescence', *Advanced Materials*, vol. 22, no. 1, pp. 77-82.

[22] Yang, C., Lee, J. K., Heeger, A. J. & Wudl, F. 2009, 'Well-defined donor-acceptor rod-coil diblock copolymers based on P3HT containing C60: The morphology and role as a surfactant in bulk-heterojunction solar cells', *Journal of Materials Chemistry*, vol. 19, no. 30, pp. 5416-23.

[23] Iovu, M. C., Rockford Craley, C., Jeffries-El, M., Krankowski, A. B., Zhang, R., Kowalewski, T. & McCullough, R. D. 2007, 'Conducting regioregular polythiophene block copolymer nanofibrils synthesized by reversible addition fragmentation chain transfer polymerization (RAFT) and Nitroxide Mediated Polymerization (NMP)', *Macromolecules*, vol. 40, no. 14, pp. 4733-5.

[24] Natansohn, Almeria 1989, 'Two-dimensional NMR spectra of poly(N-vinylcarbazole)', *Journal of Polymer Science Part A: Polymer Chemistry*, vol. 27, no. 13, pp. 4257-65.

[25] Karali, A., Froudakis, G. E., Dais, P. & Heatley, F. 2000, 'Complete assignment of 1H and 13C NMR spectra of poly(N-vinylcarbazole)', *Macromolecules*, vol. 33, no. 8, pp. 3180-3.

[26] Segalman, R. A., Hexemer, A. & Kramer, E. J. 2003, 'Edge effects on the order and freezing of a 2D array of block copolymer spheres', *Physical Review Letters*, vol. 91, no. 19, pp. 196101/1-4.

[27] Bednář, B., Karásek, L. & Pokorný, J. 1996, 'Nonradiative energy transfer studies of block copolymers in selective solvents', *Polymer*, vol. 37, no. 23, pp. 5261-8.

[28] Procházka, K., Bednář, B., Mukhtar, E., Svoboda, P., Trněná, J. & Almgren, M. 1991, 'Nonradiative energy transfer in block copolymer micelles', *Journal of Physical Chemistry*, vol. 95, no. 11, pp. 4563-8.

[29] Hu, D., Yu, J., Padmanaban, G., Ramakrishnan, S. & Barbara, P. F. 2002, 'Spatial Confinement of Exciton Transfer and the Role of Conformational Order in Organic Nanoparticles', *Nano Letters*, vol. 2, no. 10, pp. 1121-4.

Publication

1. Mihee Heo, Jonggi Kim, Jin Young Kim, Changduk Yang "**A first approach to white organic electroluminescence device from a single rod-coil poly[thiophene-block-(N-vinylcarbazole)] diblock copolymer**" *Macromolecular Rapid Communication* 2010, 31, 2047-2052 (Published)

2. Shuhei Yamada**,** Seijung Park**,** Suhee Song**,** Mihee Heo**,** Joo Young Shim**,** Youngeup Jin**,** Il Kim**,** Heesoo Lee**,** Kyungmee Lee**,** Kohji Yoshinaga**,** Jin Young Kim**,** Hongsuk Suh "**Synthesis and characterization of fluorene-carbazole and fluorene-phenothiazine copolymers with carbazole and oxadiazole pendants for organic light emitting diodes**" *Polymer* 2010, 51, 6174-6181 (Published)

3. Dong Wook Lee, Tae-Keun Hong, Dongwoo Kang, Jisook Lee, Mihee Heo, Jin Young Kim, Byeong-Su Kim and Hyeon Suk Shin "**Highly controllable transparent and conducting thin films using layer-by-layer assembly of oppositely charged reduced graphene oxides**" *Journal of Materials Chemistry* 2011, 21, 3438-3442 (Published)

4. Mihee Heo, Heesook Cho, Jae-Woo Jung, Jong-Ryul Jeong, Soojin Park, Jin Young Kim "**High-performance organic optoelectronic devices enhanced by surface plasmon resonance**" (Submitted)

5. Jieun Yang, Mihee Heo, Hyo Joong Lee, Su-Moon Park, Jin Young Kim, Hyeon Suk Shin " **Reduced graphene oxide (rGO)-wrapped fullerene (C_{60}) wires**" (Submitted)

Presentation

International

1. Mihee Heo, Jonggi Kim, Changduk Yang, Jin Young Kim "**White Light Emitting Polymer Devices Based on Poly(N-vinylcarbazole)(PVK) and Poly(3-hexylthiophene)(P3HT) Block Copolymers**" ICSM 2010 Kyoto, Japan , July 4-9.

Domestic

1. Mihee Heo, Jonggi Kim, Changduk Yang, Jin Young Kim "**White Light Emitting Polymer Devices Based on Poly(N-vinylcarbazole)(PVK) and Poly(3-hexylthiophene)(P3HT) Block Copolymers**" The Polymer Society of Korea 2010, Daejeon, April 8-9.

2. Mihee Heo, Jonggi Kim, Changduk Yang, Jin Young Kim "**A First Approach to White Organic Electroluminescence Device from a Single Rod-Coil Poly(thiophene-*block*-*N*-vinylcarbazole) Diblock Copolymer**" The Physics Society of Korea 2010, Ulsan, June 18.

3. Mihee Heo, Heesook Cho, Soojin Park, Jin Young Kim "**Plasmon-Enhanced Light Absorption and Efficiency via Self-Assembled Diblock Copolymer Template of Alloy Metal Nanoparticles**" The Polymer Society of Korea 2010, Daegu, October 7-8.

4. Mihee Heo, Heesook Cho, Soojin Park, Jin Young Kim "**High-Performance Organic Optoelectronic Devices Enhanced by Surface Plasmon Resonance**" The Polymer Society of Korea 2011, Daejeon, April 7-8.

Acknowledgement

It is a pleasure to thank the many people who have made the completion of this research project possible. At the beginning of my research program, I had to spend much time learning and understanding the research system due to my lack of experience and knowledge. However, after two long years, I have finished my MS studies successfully with the support of many people. Foremost among them, I would like to sincerely thank my advisor, Prof. Jin Young Kim, for his patience and guidance during my graduate studies with his trust and belief in me. I am also thankful and would like to acknowledge my committee members, Prof. Changduk Yang, Prof. Soojin Park, who deserve my deepest appreciation for their undivided help and support in providing professional discussions and collaboration opportunities. In addition, Prof. Yongseok Jun and Prof. Myoung Hoon Song deserve my heartfelt for being abundantly helpful and offering invaluable assistance, support, and encouragement.

I would like to express my gratefulness for the tremendous amount of assistance from my Next Generation Energy Laboratory members, Gi-Hwan Kim, Hyo Sung Choi, Myoung Hee Yun, Seojin Ko, Taehyo Kim, Hye-Rim Yeom, and Hyun Seok Shim. Whatever happiness I have felt at UNIST can be, in one way or another, traced to UMGs, Jeong-il, Jong Sang, Young Sim, Myoung Hee, Seo-Yoon, Heejin, Jason, and last but not least, Sang-Ha and Bo Ram. I will never forget the precious memories with you guys! Also, I give my sincerest thanks to ‘Solarino’ for their overwhelming kindness and hospitality. Moreover, I could not have completed my graduate degree without the support and love from my friends, Eun Jeong and Seong Hui.

Finally, I wish to express my love and gratitude to my family whom have provided great mental support during this journey. It was truly with their endless love and encouragement that I could come this far. The time at UNIST has been a great part of my life, and the knowledge and memories obtained here will be forever cherished and unforgotten.